CHAPTER 5

1,3,4-oxadiazole based unsymmetrical liquid crystals

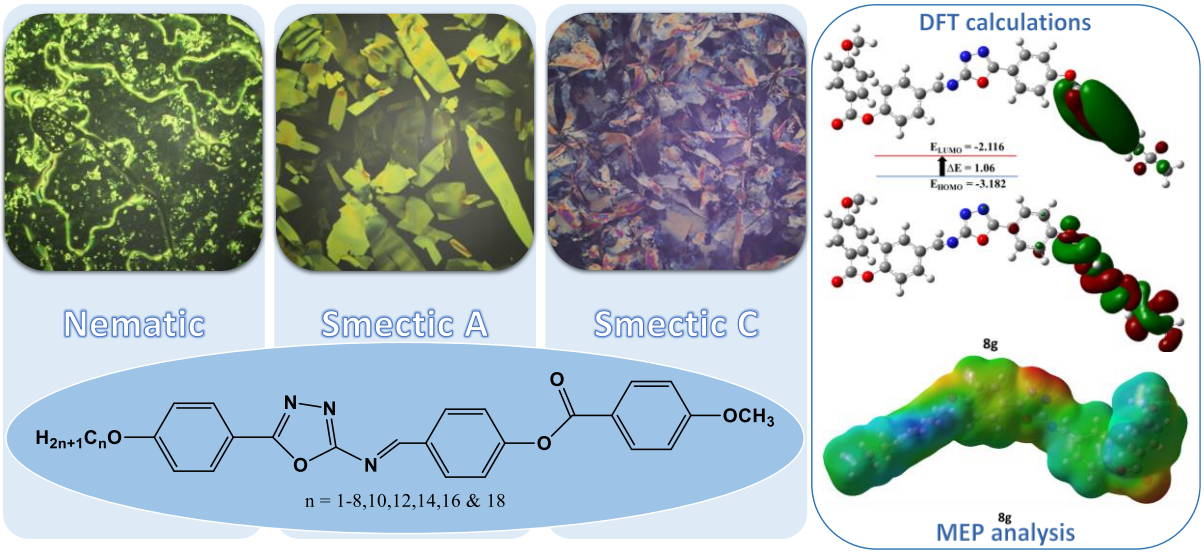

5.1. Introduction

Heterocycles hold significant position as fundamental units in LCs because of their unique structural and electronic properties. The incorporation of heterocyclic rings into liquid crystal molecules imparts distinctive characteristics, influencing the mesomorphic behaviour and performance of these materials [1,2]. The versatility of heterocycles allows for the design of liquid crystals with tailored properties, which opens up new possibilities for innovative applications in fields like improved materials, displays, and sensors [3–6]. These materials demonstrate significant promise for applications in spatial light modulation [7], organic thin-film transistors [8], all-optical signal processing, storage of optical data [9], as well as fluorophore utilized for recognition and examination of biomolecules [10], etc.

Aromatic-substituted 1,3,4-oxadiazoles find extensive use owing to their electron-deficient nature, high photoluminescence quantum yield and exceptional thermal and chemical stabilities [11]. Significant focus has been directed towards 2,5-disubstituted 1,3,4-oxadiazole among heterocyclic mesogens, attributed to their diverse mesophases and remarkable thermal stability [12–17]. The commonly employed synthetic routes for 1,3,4-oxadiazole include thermal or acid-catalysed cyclization of diacylhydrazines [18,19], oxidation of acyl hydrazones [20] and oxidative cyclization of semicarbazones [21]. The 1,3,4-oxadiazole unit transmits a huge lateral dipole beginning at O to the core of the N–N bond (3.04 D) [22] **(Figure 5.1)**.

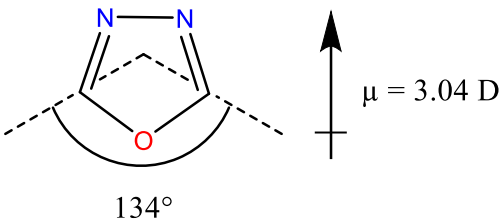

Figure 5.1: Bond angle and dipole moment of 1,3,4-oxadiazole

Early instances can be found back in 1989, when Chudgar et al [23] first described a series of mesogenic 1,3,4-oxadiazoles, exhibiting a monotropic nematic phase with elevated clearing temperatures **(Figure 5.2 (a))**.

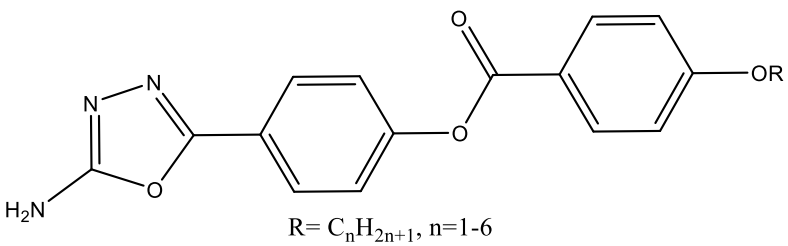

Figure 5.2 (a): First reported liquid crystalline 1,3,4-oxadiazoles

After that, many 1,3,4-oxadiazoles based calamitic liquid crystals have been reported showing variety of mesophases, including nematic, smectic A, smectic C, etc. [24–27]. Some chiral oxadiazoles have also been synthesized, showing chiral mesophase, blue phase and banana phase [28,29] **(Figure 5.2 (b** and **c))**.

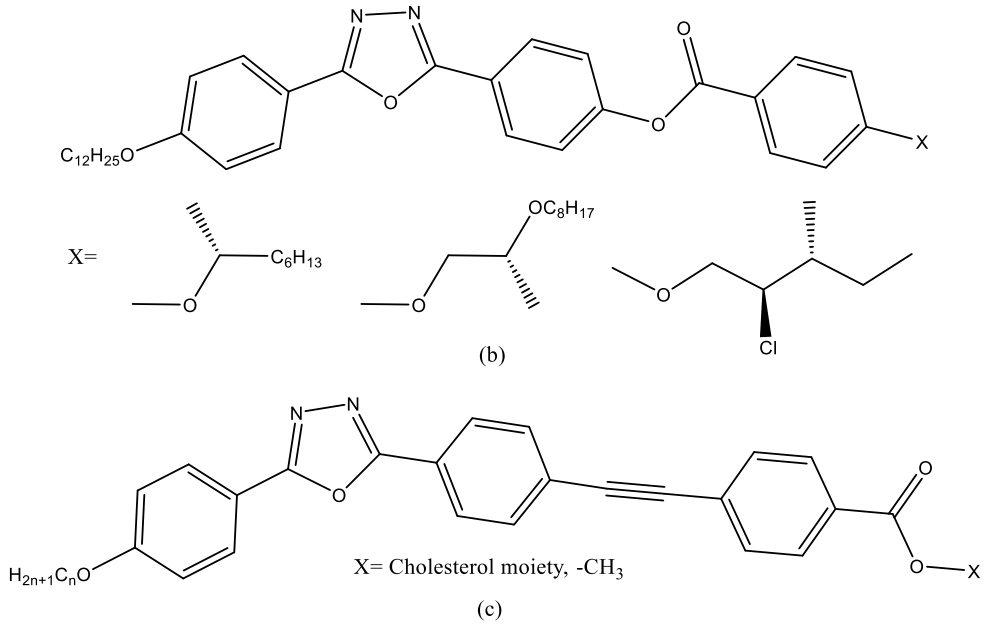

Figure 5.2 (b and **c):** Some chiral LC oxadiazoles

Efforts have been made in the synthesis and characterization of probable candidates for 1,3,4-oxadiazole based biaxial nematic liquid crystal [30–33] **(Figure 5.2 (d))**. Also, many oxadiazoles based discotic liquid crystals, LC dimer and polymers have been reported so far [34–41].

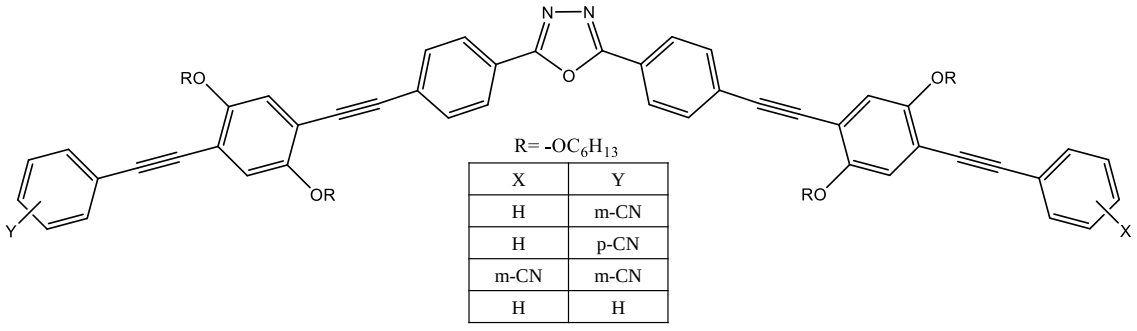

X	Y
H	m-CN
H	p-CN
m-CN	m-CN
H	H

Figure 5.2 (d): 1,3,4-oxadiazole based biaxial nematic liquid crystal

In the present study, we have synthesized a new homologous series of 1,3,4-oxadiazole based mesogenic Schiff's base derivatives containing ester linkage and terminal alkoxy chain varying from methyl to n-octadecyl. The mesomorphic characteristics of these liquid crystals were examined using DSC and POM and are correlated to the length of alkoxy groups. Also, the photoluminescence and quantum yield were studied in detail. To explore the scope of

mesogenic characteristics, the structure-property relationship of current liquid crystalline derivatives was discussed.

5.2. Experimental

5.2.1. Materials

1,1-Diphenyl-2-picrylhydrazyl (for antioxidant assay) was purchased from TCI Chemicals, Japan. p-Anisic acid, thionyl chloride, anhydrous pyridine, n-alkyl bromides, potassium carbonate, semicarbazide hydrochloride, glacial acetic acid, bromine, etc. were purchased from Loba Chemie Pvt. Ltd., India. Acetone, methanol and ethanol underwent drying treatment with standard methods. All remaining solvents and reagents were of AR grade and used without additional purification.

5.2.2. Techniques and measurements

Standard spectroscopic techniques were employed to determine the structures of the synthesized compounds. Thin-layer chromatography (TLC) was performed on silica gel plates (Merck). FT-IR spectra were recorded on a Bruker spectrometer as KBr pellets. ^{1}H NMR and ^{13}C NMR spectral data were recorded on an Avance Bruker 400 spectrometer (400 MHz) with deuterated chloroform ($CDCl_3$) as solvent and TMS as an internal standard. The polarised optical microscopy (POM) study was observed with a Nikon Eclipse *Ci*-Pol microscope equipped with a Linkam (Linkam, Surrey, England) heating stage. Phase transition temperatures and thermodynamic parameters were determined by using differential scanning calorimetry (DSC-822, Mettler Toledo, with Stare software). The heating as well as cooling rates were 10°C/min. The instrument underwent calibration using indium as the standard. The thermal stability of the compounds was recorded using a thermogravimetry analyser (TGA-50, Shimadzu, Japan) with 3-7 mg of the sample in a platinum pan at a heating rate of 10°C/min. Thermo Finnigan's (Flash 1112 series EA) CHN analyser was used to carry out elemental analyses. Absorbance was recorded using a Shimadzu UV-1800 spectrophotometer (Japan). Photoluminescence and quantum yields (Φ_{PL}) were measured using a Shimadzu RF 6000 Spectro fluorophotometer (Japan). Gaussian 09, revision A.02 software was utilized for DFT calculations.

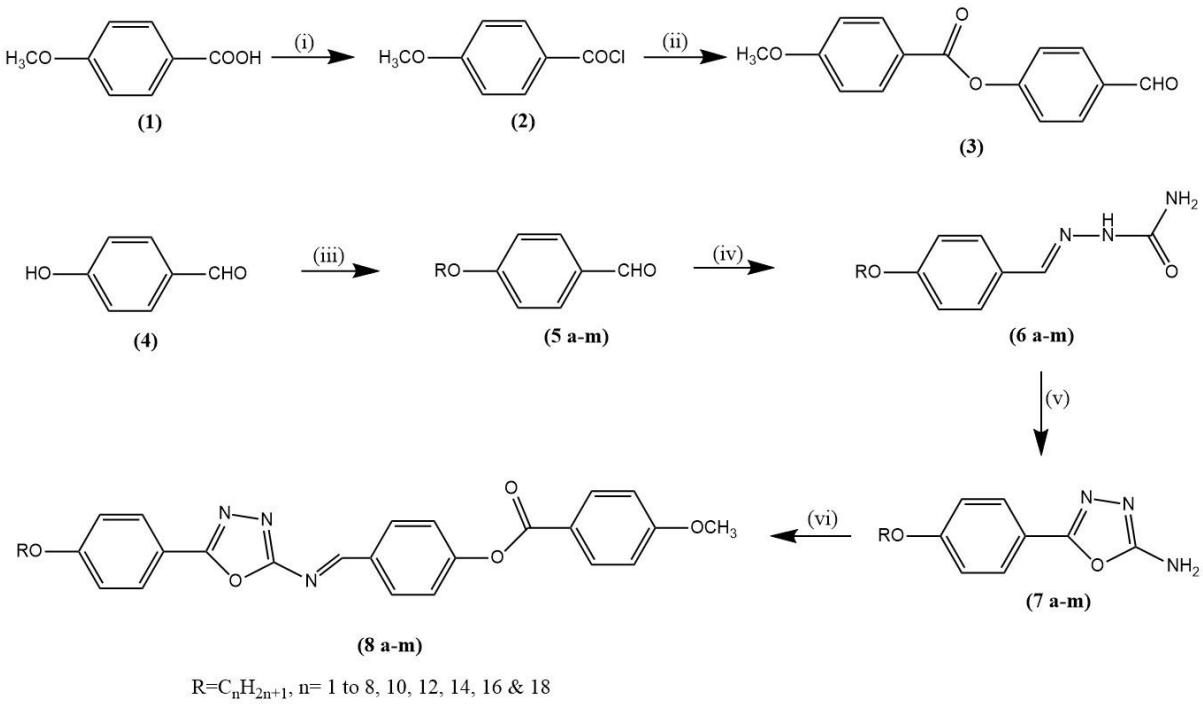

Scheme 5.1: Synthetic route for final derivatives (8 a-m). Reagents and conditions; (i) $SOCl_2$, reflux, 3-4 h, (ii) p-hydroxybenzaldehyde, pyridine, 60-70°C, 2-3 h, (iii) n-alkyl bromide, K_2CO_3, dry acetone, 80°C, 10-12 h, (iv) semicarbazide HCl, EtOH/water, 5 minutes, (v) Glac. HAc, Br_2, strring 3-4 h, (vi) Ethanol, glac. HAc, reflux, 10-12 h

5.2.3. Synthesis and characterisation

The synthetic routes of the mesogenic Schiff's base are shown in Scheme 5.1.

5.2.3.1. Synthesis of 4-(4′-methoxybenzoyloxy) benzaldehyde ***(3)***

4-methoxybenzoylchloride **(2)** was synthesized using p-anisic acid by the modified method of Dave and Vora [42]. 4-(4′-methoxybenzoyloxy) benzaldehyde was synthesised according to reported procedure [43].

5.2.3.2. Synthesis of 4-n-alkoxy benzaldehydes ***(5 a-m)***

4-n-Alkoxy benzaldehydes were synthesised by the previously reported procedures [44,45]. In a three-necked round-bottomed flask, 4-hydroxybenzaldehyde (0.1 mol) **(4)**, anhy. K_2CO_3 (0.12 mol), and dry acetone (150 mL) were combined. The reaction mixture was heated and stirred at 80°C. The appropriate alkyl bromide (0.12 mol) was added dropwise over 1 h to the warm solution. The mixture was further heated at 80°C for 8-12 h. After cooling to room

temperature, the mixture was diluted with water (150 mL). The aqueous phase was extracted with diethyl ether (3 × 100 mL). The combined organic layer was washed with aq. NaOH (10% mol), water, and dried with Na_2SO_4. After solvent evaporation on a rotary evaporator, the resulting products were obtained as pale-yellow oils, subsequently used without purification.

5.2.3.3. Synthesis of 4-n-alkoxy benzaldehyde semicarbazone ***(6 a-m)***

4-n-alkoxy benzaldehydes (0.01 mol) **(5a-m)** was dissolved in 10 ml of ethanol. Water was added until the solution became faintly turbid, and the turbidity was removed with a few drops of ethanol. Then, semicarbazide hydrochloride (0.03 mol) and 1.5 g of anhy. sodium acetate (0.06 mol) was added. The mixture was vigorously shaken, and the RBF was placed in boiling water bath for 5 min. The RBF was removed from the bath, allowed to cool, and the crystals of the semicarbazone were isolated by filtration. The obtained crystals were recrystallized from 50% ethanol [46].

5.2.3.4. Synthesis of 5-(4'-n-alkoxy phenyl)-2-amino-1,3,4-oxadiazole ***(7 a-m)***

Bromine (1 ml) in glac. acetic acid (10 ml) was added to a stirred slurry of 4-n-alkoxy benzaldehyde semicarbazone (0.01 mol) **(6a-m)** and anhy. sodium acetate (0.06 mol) in glac. acetic acid (10 ml) contained in a 150 ml flat bottom flask and stirred for 30 minutes at room temperature. Due to exothermic reaction, the mixture became warm and rapidly became colourless. Subsequently, mixture was poured in water and the separated solid was filtered and dried. All the amino oxadiazoles were recrystallized from the mixture of alcohol and glacial acetic acid [23,47].

5.2.3.5. Synthesis of 5-(4-n-alkoxy phenyl)-2-(4-(4'-methoxy benzoyloxy)) benzylideneamino-1,3,4-oxadiazoles ***(8 a-m)***

A mixture containing aldehyde **(3)** (0.002 mol), 1,3,4-oxadiazoles **(7a-m)** (0.002 mol), a few drops of glacial acetic acid and 25 ml of EtOH was refluxed with continuous stirring for 10-12 hours. Subsequently, the solvent was evaporated, and resulting remnants was repeatedly crystallized using alcohol until a consistent transition temperature was achieved, yielding yellow crystals. Yield: 65–70 %.

Compound 8a: Off white crystalline solid, yield: 80.4%, IR (KBr, ν_{max} , cm^{-1}): 3045, 2966, 2854, 2846, 1741, 1624, 1581, 1508, 1241, 1215, 844; ^{1}H-NMR ($CDCl_3$, 400 MHz): δ(ppm) = δ8.99 (s, 1H, -CH=N), δ6.80-8.13 (m, 12 H, Ar-H), δ3.81 (s, 6H, $-OCH_3$); ^{13}C NMR

($CDCl_3$, 400MHz): δ(ppm) = 165.8, 165.2 (-COO), 164.5 (C_5-1,3,4-oxadiazole), 160.6, 160.0 (-CH=N-), 155.7, 135.90, 133.2, 131.3, 129.63, 122.5, 121.71, 118.4, 115.91, 114.8, 114.2, 55.8; Elemental analysis: calculated for $C_{24}H_{19}N_3O_5$(%): C, 67.13; H, 4.46; N, 9.79; found: C, 66.83; H, 4.74; N, 10.01.

Compound 8b: Off white crystalline solid, yield: 82.6%, IR (KBr, ν_{max} , cm^{-1}): 3044, 2970, 2856, 2842, 1741, 1626, 1582, 1506, 1240, 1214, 846; ^{1}H-NMR ($CDCl_3$, 400 MHz): δ(ppm) = δ8.98 (s, 1H, -CH=N), δ6.89-8.13 (m, 12 H, Ar-H), δ4.05 (m, 2H, -OC<u>H</u>$_2$-), δ3.81 (s, 3H, -OCH_3), δ1.34 (t, 3H, -CH_2C<u>H</u>$_3$); ^{13}C NMR ($CDCl_3$, 400MHz): δ(ppm) = 165.8, 165.2 (-COO), 164.5 (C_5-1,3,4-oxadiazole), 160.0 (-CH=N-), 159.40, 154.9, 133.21, 131.37, 129.60, 122.54, 121.73, 117.74, 115.56, 114.92, 114.21, 64.60, 55.82, 14.83; Elemental analysis: calculated for $C_{25}H_{21}N_3O_5$(%): C, 67.71; H, 4.77; N, 9.48; found: C, 67.98; H, 4.95; N, 9.70.

Compound 8c: Off white crystalline solid, yield: 82%, IR (KBr, ν_{max} , cm^{-1}): 3034, 2976, 2850, 2844, 1742, 1624, 1576, 1510, 1244, 1218, 840; ^{1}H-NMR ($CDCl_3$, 400 MHz): δ(ppm) = δ8.99 (s, 1H, -CH=N), δ6.89-8.19 (m, 12 H, Ar-H), δ4.02 (m, 2H, -OC<u>H</u>$_2$-), δ3.81 (s, 3H, -OCH_3), δ1.76 (m, 2H, -C<u>H</u>$_2$$CH_3$), δ1.01 (t, 3H, -$CH_2C$<u>H</u>$_3$) ; ^{13}C NMR ($CDCl_3$, 400MHz): δ(ppm) = 165.80, 165.21 (-COO), 164.52 (C_5-1,3,4-oxadiazole), 160.0 (-CH=N-), 159.40, 154.9, 133.22, 131.36, 129.60, 122.56, 121.71, 117.76, 115.50, 114.91, 114.21, 69.35, 55.80, 22.68, 10.41; Elemental analysis: calculated for $C_{26}H_{23}N_3O_5$(%): C, 68.26; H, 5.07; N, 9.19; found: C, 68.07; H, 5.36; N, 9.42.

Compound 8d: Off white crystalline solid, yield: 78.5%, IR (KBr, ν_{max} , cm^{-1}): 3038, 2978, 2849, 2842, 1740, 1627, 1578, 1516, 1245, 1222, 844; ^{1}H-NMR ($CDCl_3$, 400 MHz): δ(ppm) = δ8.99 (s, 1H, -CH=N), δ6.89-8.02 (m, 12 H, Ar-H), δ4.00 (m, 2H, -OCH_2-), δ3.81 (s, 3H, -OCH_3), δ1.74 (m, 2H, -C<u>H</u>$_2$$CH_2$-), δ1.48 (m, 2H, -C<u>H</u>$_2$$CH_3$), δ0.99 (s, 3H, -$CH_2C$<u>H</u>$_3$) ; ^{13}C NMR ($CDCl_3$, 400MHz): δ(ppm) = 165.82, 165.22 (-COO), 164.54 (C_5-1,3,4-oxadiazole), 160.03 (-CH=N-), 159.41, 154.96, 133.24, 131.34, 129.58, 122.46, 121.74, 117.72, 115.50, 114.92, 114.22, 68.42, 55.86, 31.82, 19.04, 14.16 ; Elemental analysis: calculated for $C_{27}H_{25}N_3O_5$(%): C, 68.78; H, 5.34; N, 8.91; found: C, 68.50; H, 5.02; N, 9.18.

Compound 8e: Off white crystalline solid, yield: 76.5%, IR (KBr, ν_{max} , cm^{-1}): 3042, 2970, 2841, 2837, 1742, 1626, 1575, 1522, 1242, 1220, 844; ^{1}H-NMR ($CDCl_3$, 400 MHz): δ(ppm) = δ8.99 (s, 1H, -CH=N), δ6.91-8.19 (m, 12 H, Ar-H), δ4.06 (m, 2H, -OCH_2-), δ3.81 (s, 3H, -OCH_3), δ1.78 (m, 2H, -C<u>H</u>$_2$$CH_2$-), δ1.40 (m, 4H, -C<u>H</u>$_2$C<u>H</u>$_2$$CH_3$), δ0.91 (s, 3H, -$CH_2C$<u>H</u>$_3$) ; ^{13}C NMR ($CDCl_3$, 400MHz): δ(ppm) = 165.82, 165.20 (-COO), 164.54 (C_5-1,3,4-oxadiazole), 160.02 (-CH=N-), 159.40, 154.94, 133.26, 131.32, 129.58, 122.46, 121.74, 17.74,

115.54, 114.92, 114.21, 68.74, 55.86, 29.30, 22.79, 14.12 ; Elemental analysis: calculated for $C_{28}H_{27}N_3O_5$(%): C, 69.26; H, 5.61; N, 8.65; found: C, 69.04; H, 5.88; N, 8.91.

Compound 8f: Off white crystalline solid, yield: 77.4%, IR (KBr, ν_{max} , cm^{-1}): 3037, 2947, 2866, 2850, 1742, 1626, 1579, 1508, 1247, 1217, 842; ^{1}H-NMR ($CDCl_3$, 400 MHz): δ(ppm) = δ8.96 (s, 1H, -CH=N), δ6.96-8.20 (m, 12 H, Ar-H), δ4.01 (t, 2H, -OC<u>H</u>$_2$-CH_2-), δ3.89 (s, 3H, -OCH_3), δ0.86-1.88 (m for 11H, -CH_2 and -CH_3 of alkoxy chain); ^{13}C NMR ($CDCl_3$, 400MHz): δ(ppm) = 165.80, 165.28 (-COO), 164.59 (C_5-1,3,4-oxadiazole), 160.0 (-CH=N-), 159.4, 154.93, 135.90, 132.46, 131.26, 122.63, 120.81, 119.5, 117.0, 116.6, 114.45, 68.40, 54.8, 29.52, 28.04, 22.04, 14.03; Elemental analysis: calculated for $C_{29}H_{29}N_3O_5$(%): C, 69.72; H, 5.85; N, 8.41; found: C, 69.45; H, 6.09; N, 8.73.

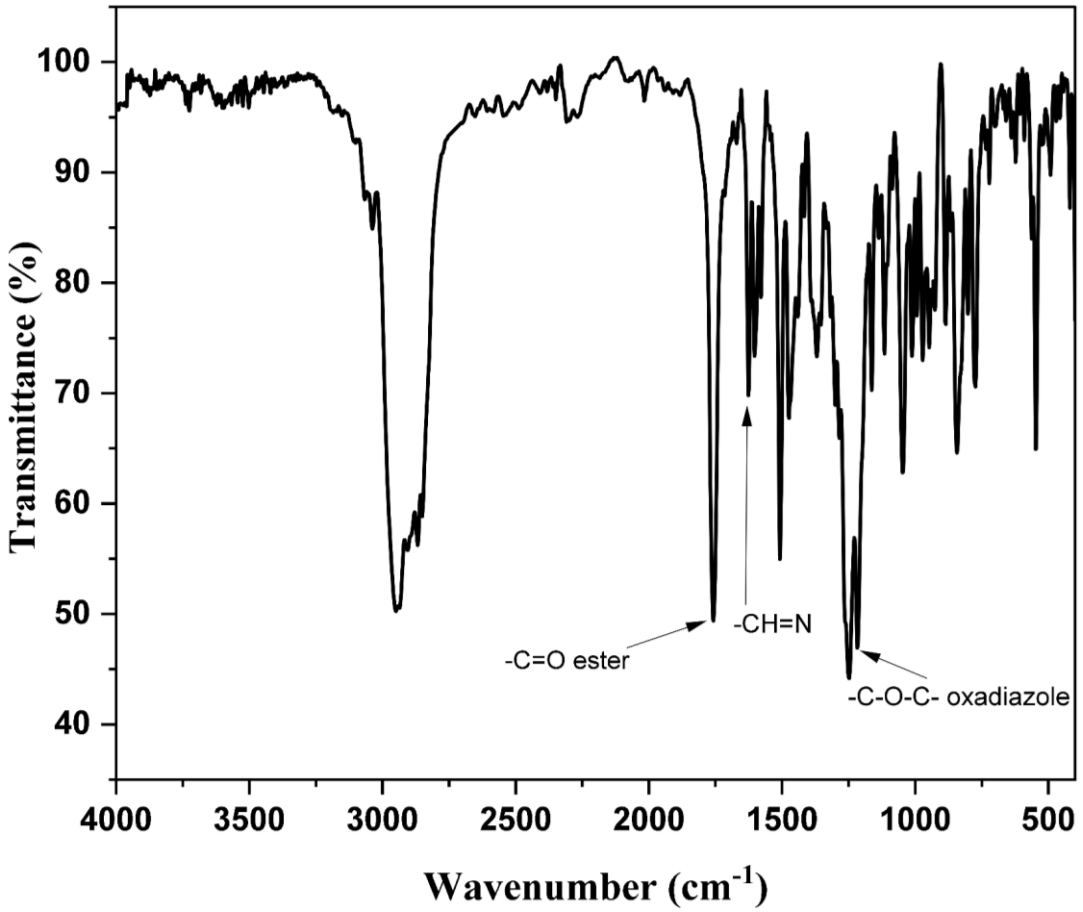

Figure 5.3 (a): FT-IR spectra of **Compound 8f**

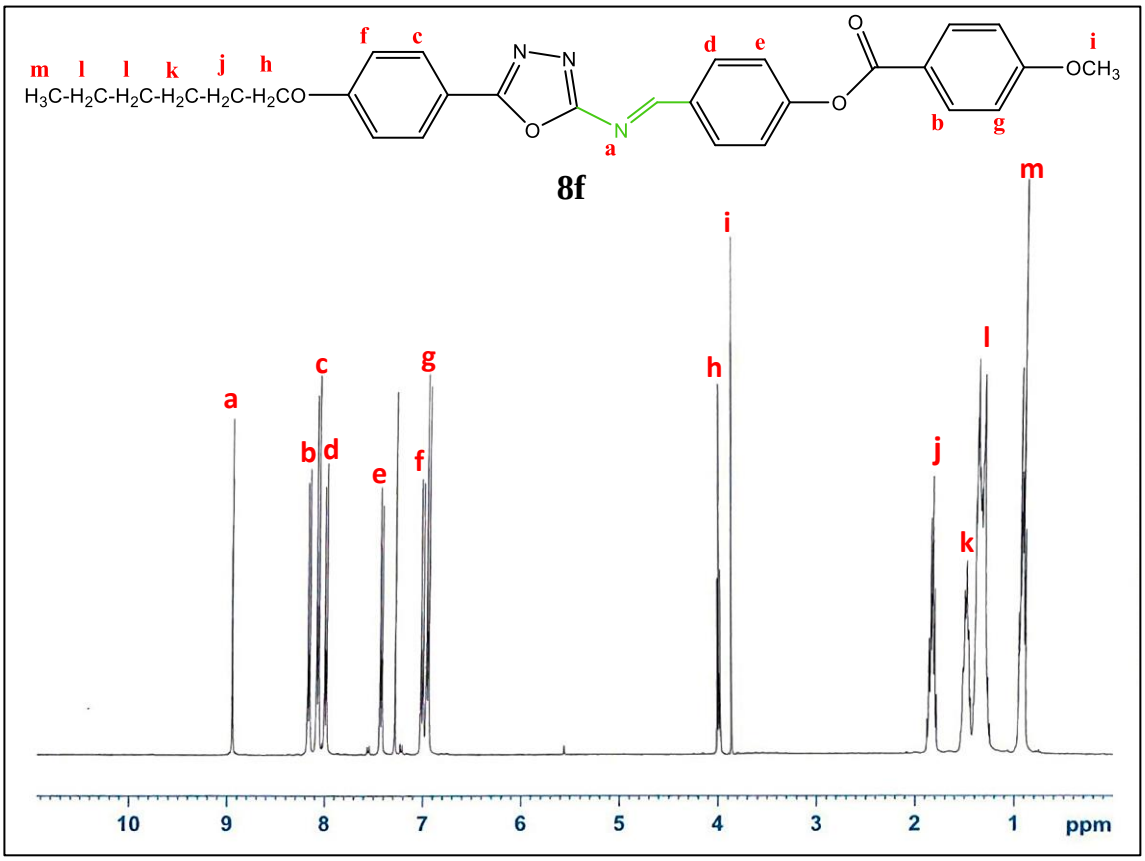

Figure 5.3 (b): ^{1}H-NMR spectra of **Compound 8f**

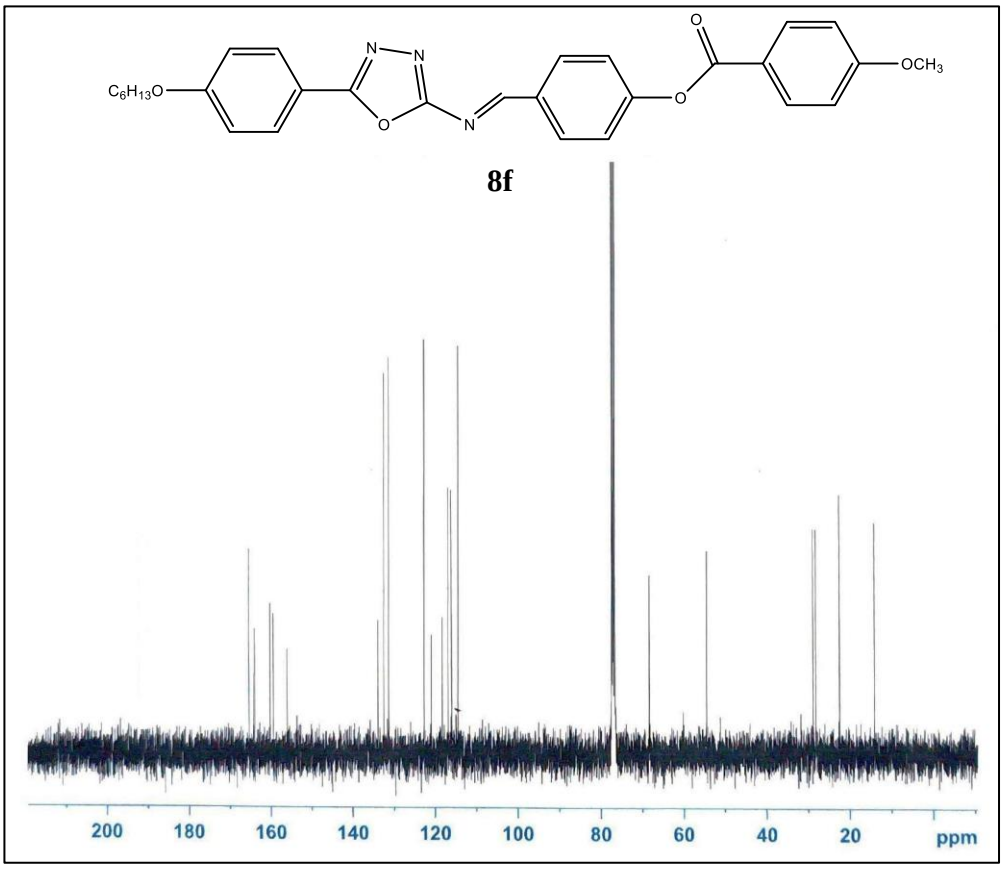

Figure 5.3 (c): ^{13}C-NMR spectra of **Compound 8f**

Compound 8g: Off white crystalline solid, yield: 78.0%, IR (KBr, ν_{max} , cm^{-1}): 3036, 2942, 2860, 2850, 1741, 1626, 1577, 1506, 1245, 1217, 836; ^{1}H-NMR ($CDCl_3$, 400 MHz): δ(ppm) = δ8.99 (s, 1H, -CH=N), δ6.89-8.13 (m, 12 H, Ar-H), δ4.04 (t, 2H, -OC<u>H</u>$_2$-CH_2-), δ3.89 (s, 3H, -OCH_3), δ0.88-1.74 (m for 13H, -CH_2 and -CH_3 of alkoxy chain); ^{13}C NMR ($CDCl_3$, 400MHz): δ(ppm) = 165.80, 165.22 (-COO), 164.56 (C_5-1,3,4-oxadiazole), 160.0 (-CH=N-), 159.4, 154.78, 135.23, 131.32, 129.64, 122.59, 121.78, 117.70, 115.06, 114.95, 68.45, 54.76, 31.80, 29.66, 29.31, 25.92, 22.78, 14.12; Elemental analysis: calculated for $C_{30}H_{31}N_3O_5$(%): C, 70.16; H, 6.08; N, 8.18; found: C, 69.94; H, 6.19; N, 8.23.

Compound 8h: Off white crystalline solid, yield: 73.8%, IR (KBr, ν_{max} , cm^{-1}): 3042, 2936, 2845, 2831, 1742, 1626, 1575, 1506, 1242, 1214, 844; ^{1}H-NMR ($CDCl_3$, 400 MHz): δ(ppm) = δ8.99 (s, 1H, -CH=N), δ6.89-8.13 (m, 12 H, Ar-H), δ4.06 (t, 2H, -OC<u>H</u>$_2$-CH_2-), δ3.89 (s, 3H, -OCH_3), δ0.88-1.74 (m for 15H, -CH_2 and -CH_3 of alkoxy chain); ^{13}C NMR ($CDCl_3$, 400MHz): δ(ppm) = 165.80, 165.22 (-COO), 164.55 (C_5-1,3,4-oxadiazole), 160.0 (-CH=N-), 159.41, 154.76, 135.24, 131.33, 129.62, 122.58, 121.76, 117.72, 115.06, 114.96, 68.70, 55.80, 31.92, 29.77, 29.68, 29.54, 25.94, 22.76, 14.11; Elemental analysis: calculated for $C_{31}H_{33}N_3O_5$(%): C, 70.57; H, 6.30; N, 7.96; found: C, 70.42; H, 6.11; N, 8.06.

Compound 8i: Off white crystalline solid, yield: 72.5%, IR (KBr, ν_{max} , cm^{-1}): 3042, 2933, 2847, 2836, 1740, 1624, 1576, 1506, 1247, 1208, 838; ^{1}H-NMR ($CDCl_3$, 400 MHz): δ(ppm) = δ9.00 (s, 1H, -CH=N), δ6.87-8.12 (m, 12 H, Ar-H), δ4.08 (t, 2H, -OC<u>H</u>$_2$-CH_2-), δ3.81 (s, 3H, -OCH_3), δ0.84-1.76 (m for 19H, -CH_2 and -CH_3 of alkoxy chain); ^{13}C NMR ($CDCl_3$, 400MHz): δ(ppm) = 165.80, 165.20 (-COO), 164.54 (C_5-1,3,4-oxadiazole), 160.0 (-CH=N-), 159.42, 154.76, 135.24, 131.32, 129.64, 122.57, 121.77, 117.74, 115.06, 114.95, 68.71, 55.79, 31.91, 29.68, 29.61, 29.48, 29.39, 29.17, 25.88, 22.72, 14.16; Elemental analysis: calculated for $C_{33}H_{37}N_3O_5$(%): C, 71.33; H, 6.71; N, 7.56; found: C, 71.04; H, 6.65; N, 7.70.

Compound 8j: White crystalline solid, yield: 75.8%, IR (KBr, ν_{max} , cm^{-1}): 3032, 2951, 2866, 2852, 1745, 1624, 1575, 1506, 1246, 1215, 831; ^{1}H-NMR ($CDCl_3$, 400 MHz): δ(ppm) = δ8.91 (s, 1H, -CH=N), δ6.89-8.19 (m, 12 H, Ar-H), δ4.08 (t, 2H, -OC<u>H</u>$_2$-CH_2-), δ3.90 (s, 3H, -OCH_3), δ0.89-1.82 (m for 23H, -CH_2 and -CH_3 of alkoxy chain); ^{13}C NMR ($CDCl_3$, 400MHz): δ(ppm) = 165.78, 165.16 (-COO), 164.66 (C_5-1,3,4-oxadiazole), 160.0 (-CH=N-), 159.33, 154.68, 133.14, 131.27, 129.66, 122.60, 121.68, 117.29, 115.42, 114.87, 68.23, 56.70, 31.89, 29.56, 29.55, 29.37, 29.31, 29.19, 29.15, 29.03, 26.00, 22.68, 14.11; Elemental analysis: calculated for $C_{35}H_{41}N_3O_5$(%): C, 72.02; H, 7.08; N, 7.20; found: C, 71.85; H, 7.27; N, 7.51.

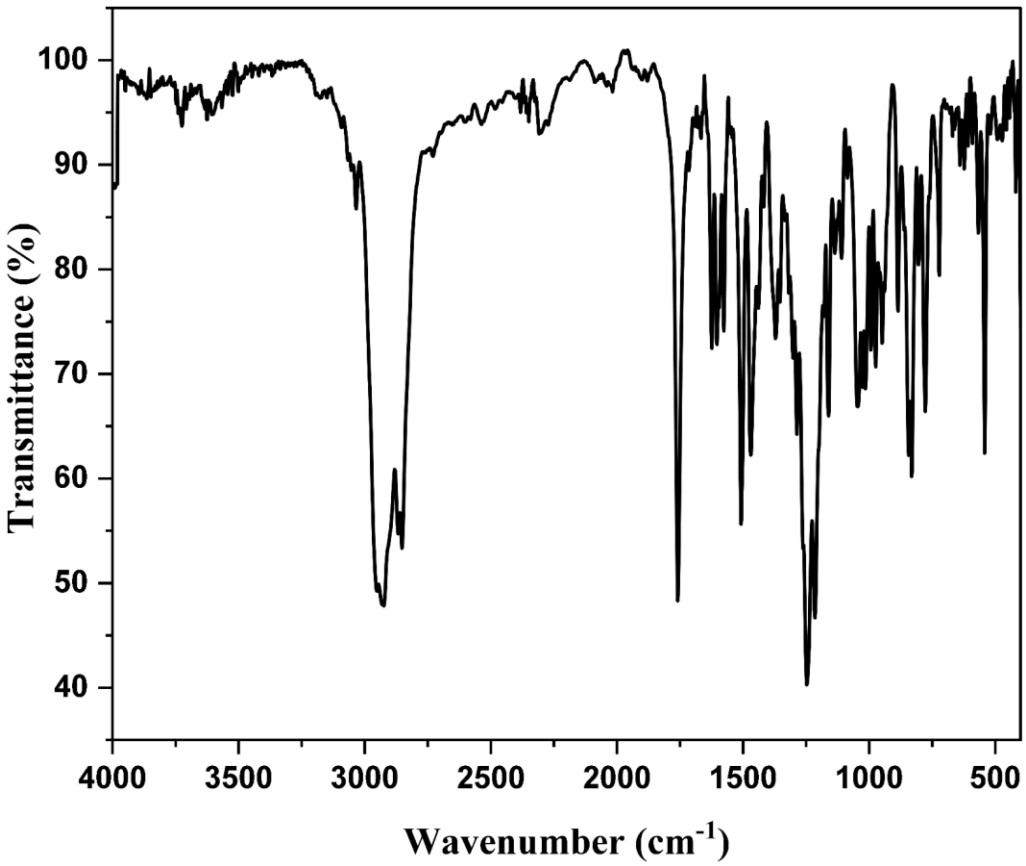

Figure 5.4 (a): FT-IR spectra of **Compound 8j**

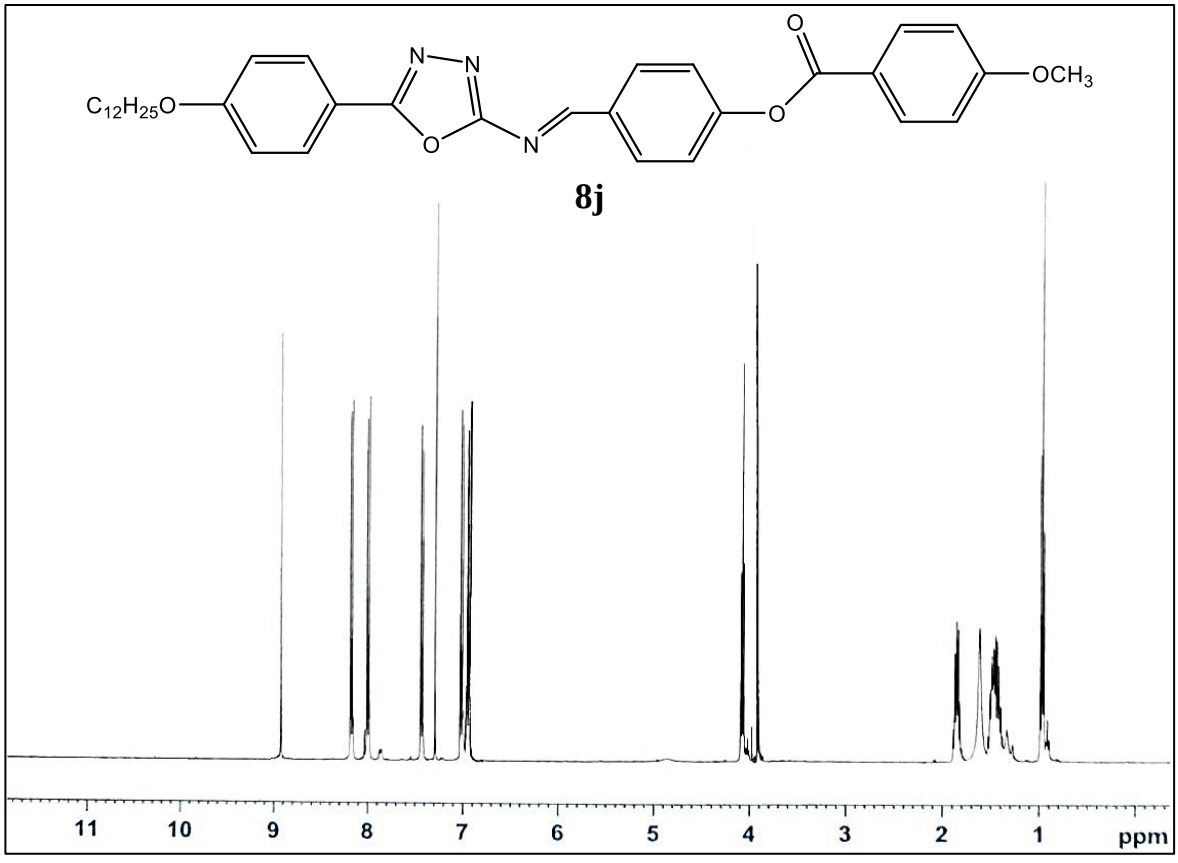

Figure 5.4 (b): ^{1}H-NMR spectra of **Compound 8j**

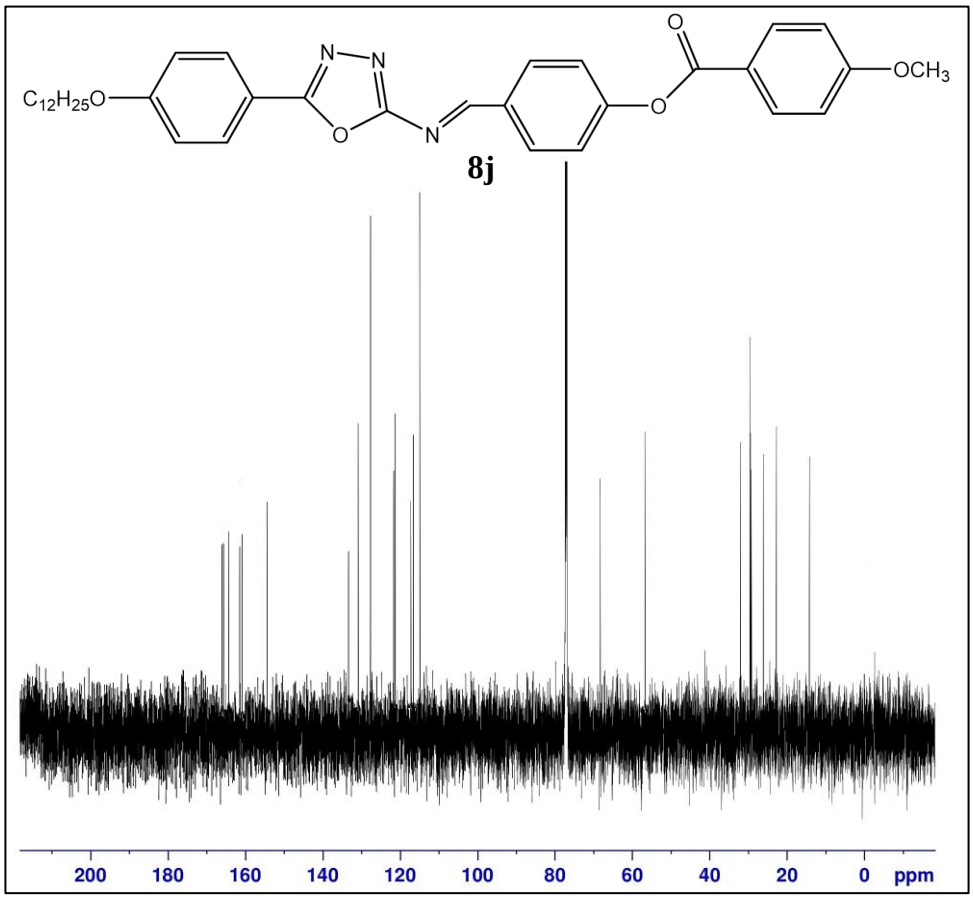

Figure 5.4 (c): ^{13}C-NMR spectra of **Compound 8j**

Compound 8k: White crystalline solid, yield: 78.0%, IR (KBr, ν_{max} , cm^{-1}): 3037, 2944, 2863, 2852, 1741, 1625, 1576, 1508, 1246, 1219, 844; ^{1}H-NMR ($CDCl_3$, 400 MHz): δ(ppm) = δ9.00 (s, 1H, -CH=N), δ6.89-8.20 (m, 12 H, Ar-H), δ4.07 (t, 2H, -OC<u>H</u>$_2$-CH$_2$-), δ3.81 (s, 3H, -OCH_3), δ0.80-1.76 (m for 27H, -CH_2 and -CH_3 of alkoxy chain); ^{13}C NMR ($CDCl_3$, 400MHz): δ(ppm) = 165.82, 165.22 (-COO), 164.50 (C_5-1,3,4-oxadiazole), 160.0 (-CH=N-), 159.42, 154.70, 134.20, 130.42, 129.66, 123.43, 119.68, 117.60, 115.12, 113.85, 68.72, 55.87, 32.13, 29.68, 29.58, 29.54, 29.39, 29.33, 29.20, 29.16, 29.03, 28.47, 24.81, 21.66, 15.49; Elemental analysis: calculated for $C_{37}H_{45}N_3O_5$(%): C, 72.64; H, 7.41; N, 6.87; found: C, 72.39; H, 7.13; N, 6.57.

Compound 8l: White crystalline solid, yield: 82.7%, IR (KBr, ν_{max} , cm^{-1}): 3042, 2945, 2860, 2848, 1744, 1626, 1578, 1508, 1248, 1216, 842; ^{1}H-NMR ($CDCl_3$, 400 MHz): δ(ppm) = δ9.00 (s, 1H, -CH=N), δ6.90-8.18 (m, 12 H, Ar-H), δ4.08 (t, 2H, -OC<u>H</u>$_2$-CH$_2$-), δ3.81 (s, 3H, -OCH_3), δ0.87-1.78 (m for 31H, -CH_2 and -CH_3 of alkoxy chain); ^{13}C NMR ($CDCl_3$, 400MHz): δ(ppm) = 165.79, 165.20 (-COO), 164.50 (C_5-1,3,4-oxadiazole), 160.0 (-CH=N-), 159.40, 154.8, 134.20, 131.26, 129.30, 122.57, 119.62, 117.64, 115.18, 114.86, 68.77, 56.67, 32.11, 31.02, 29.77, 29.71, 29.65, 29.58, 29.42, 29.38, 29.18, 29.13, 24.81, 22.73, 14.19; Elemental

analysis: calculated for $C_{39}H_{49}N_3O_5$(%): C, 73.21; H, 7.72; N, 6.57; found: C, 72.98; H, 7.57; N, 6.31.

Compound 8m: White crystalline solid, yield: 86.4%, IR (KBr, ν_{max} , cm^{-1}): 3037, 2942, 2858, 2846, 1740, 1624, 1575, 1506, 1242, 1218, 831; ^{1}H-NMR ($CDCl_3$, 400 MHz): δ(ppm) = δ9.00 (s, 1H, -CH=N), δ6.86-8.14 (m, 12 H, Ar-H), δ4.08 (t, 2H, -OC<u>H</u>$_2$-CH_2-), δ3.88 (s, 3H, -OCH_3), δ0.81-1.78 (m for 35H, -CH_2 and -CH_3 of alkoxy chain); ^{13}C NMR ($CDCl_3$, 400MHz): δ(ppm) = 165.80, 165.22 (-COO), 164.51 (C_5-1,3,4-oxadiazole), 160.1 (-CH=N-), 159.41, 153.89, 133.91, 131.34, 129.81, 124.67, 119.54, 118.32, 115.67, 114.35, 69.14, 56.04, 31.92, 29.87, 29.76, 29.68, 29.43, 29.35, 29.26, 29.20, 29.13, 29.06, 28.61, 25.18, 22.31, 14.21; Elemental analysis: calculated for $C_{41}H_{53}N_3O_5$(%): C, 73.73; H, 8.00; N, 6.29; found: C, 73.53; H, 7.86; N, 6.60.

5.3. Results and discussions

5.3.1. Structural characterisation

The final compounds **(8a-m)** were prepared by condensation of 4-(4′-methoxybenzoyloxy) benzaldehyde **(3)** with the appropriate 5-(4'-n-alkoxy phenyl)-2-amino-1,3,4-oxadiazole **(7a-m)**. The synthetic route adopted is given in Scheme 1. All the compounds in the series exhibit mesomorphic properties. The methyl to n-pentyl derivatives exhibited an enantiotropic nematic phase, while the n-hexyl to n-decyl derivatives displayed an enantiotropic SmA-N-Isotropic transition. Furthermore, the n-dodecyl to n-octadecyl homologues showed an enantiotropic SmA mesophase. Additionally, the n-hexadecyl, as well as the n-octadecyl homologue, also displayed a monotropic SmC mesophase transition during the cooling cycle. The DSC thermograms are in comparable agreement with the polarising optical microscopy. Compounds were also thermally stable up to 315-355°C as analyzed thermogravimetrically.

The FT-IR and NMR spectra, as well as the elemental analyses, are in complete agreement with the structure. In IR spectra, the compound 5-(4-n-petyloxy phenyl)-2-(4-(4′-methoxy benzoyloxy)) benzylideneamino-1,3,4-oxadiazoles **(8f)**, exhibits major IR bands (ν_{max}, cm^{-1}) at 3037 (-CH; aromatic), 2947, 2866, 2850 (-CH; aliphatic), 1745 (-C=O; ester), 1626 (-CH=N; azomethine), 1579, 1508 (-C=C-; aromatic) and 1247, 1217 (-C-O-C-; oxadiazole). The appearance of a band at 1745 cm^{-1} due to ester linkages and 1623 cm^{-1} due to azomethine

(CH=N) indicate condensation of aldehyde with amine to form Schiff base, thereby confirming the compound **8f** structure.

The proton NMR for final compound 5-(4-n-petyloxy phenyl)-2-(4-(4′-methoxy benzoyloxy)) benzylideneamino-1,3,4-oxadiazoles **(8f)** depicts signals at δ8.96 (s, 1H, -CH=N), δ6.96-8.20 (m, 12 H, Ar-H), δ4.01 (t, 2H, -OC$\underline{H_2}$-CH_2-), δ3.89 (s, 3H, -OCH_3), δ1.88-0.86 (m for 11H, -CH_2 and -CH_3 of alkoxy chain) ppm, respectively. The ^{13}C NMR spectrum of the compound **(8f)** exhibits prominent signal at δ165.2 (-C=O; ester), δ164.5 (C_5; 1,3,4-oxadiazole), δ160.0 (-CH=N; azomethine) and δ132.4-114.4 (carbons of aromatic rings) ppm thereby confirming the formation of the final compound **8f**.

The rest of the members in the series displayed similar IR and NMR (^{1}H and ^{13}C) spectra, which are outlined in the synthetic part.

5.3.2. Texture analysis

Using a POM with a heating stage, the optical textures of the Schiff's bases **8a–m** was analysed in order to identify the mesomorphic phases by observing distinctive textures. **Figure 5.5** depicts their typical textures. All of the homologues showed LC behaviour and remained stable upon repeated heating and cooling cycles.

In the series of compounds **8a-m**, the lower homologues, i.e., **8a-e**, exhibited distinctive textures resembling to the nematic (N) mesophase texture **(Figure 5.5 (a))** upon heating, which progressed to the isotropic phase. Subsequent cooling from the isotropic state resulted in the reappearance of nematic droplets textures, which then gradually combined and transformed into a nematic texture. They belong to the class of thermotropic enantiotropic nematic liquid crystals and had a unique texture that was apparent until the sample crystallised. The homologues **8f-i** on heating first exhibited a Smectic A (SmA) mesophase which on further heating transformed to nematic mesophase and persisted till the compounds became isotropic. These phases were also obtained during cooling cycles as well, showing isotropic to nematic to smectic A transition until sample crystallised. **Figure 5.5 (b)** depicts the phase transition from nematic to smectic A in cooling cycle [48]. The compounds **8j-m**, on heating cycle exhibited SmA mesophase until isotropic. Further, on cooling from isotropic phase compound **8j** and **8k** shows SmA mesophase (**Figure 5.5 (c)** showing batonnet texture of SmA phase) till compound crystallises (**Figure 5.5 (d)** showing SmA to Cr transition), revealing that both are enantiotropic SmA LCs. Moreover, compound **8l** and **8m** upon cooling first exhibits SmA mesophase and on further cooling a monotropic Smectic C (SmC) mesophase [48] **(Figure 5.5**

(e) and **(f))** is observed in addition to the SmA mesophase until crystallisation. Although not observed clearly in DSC thermograms these SmC mesophases were observed using POM.

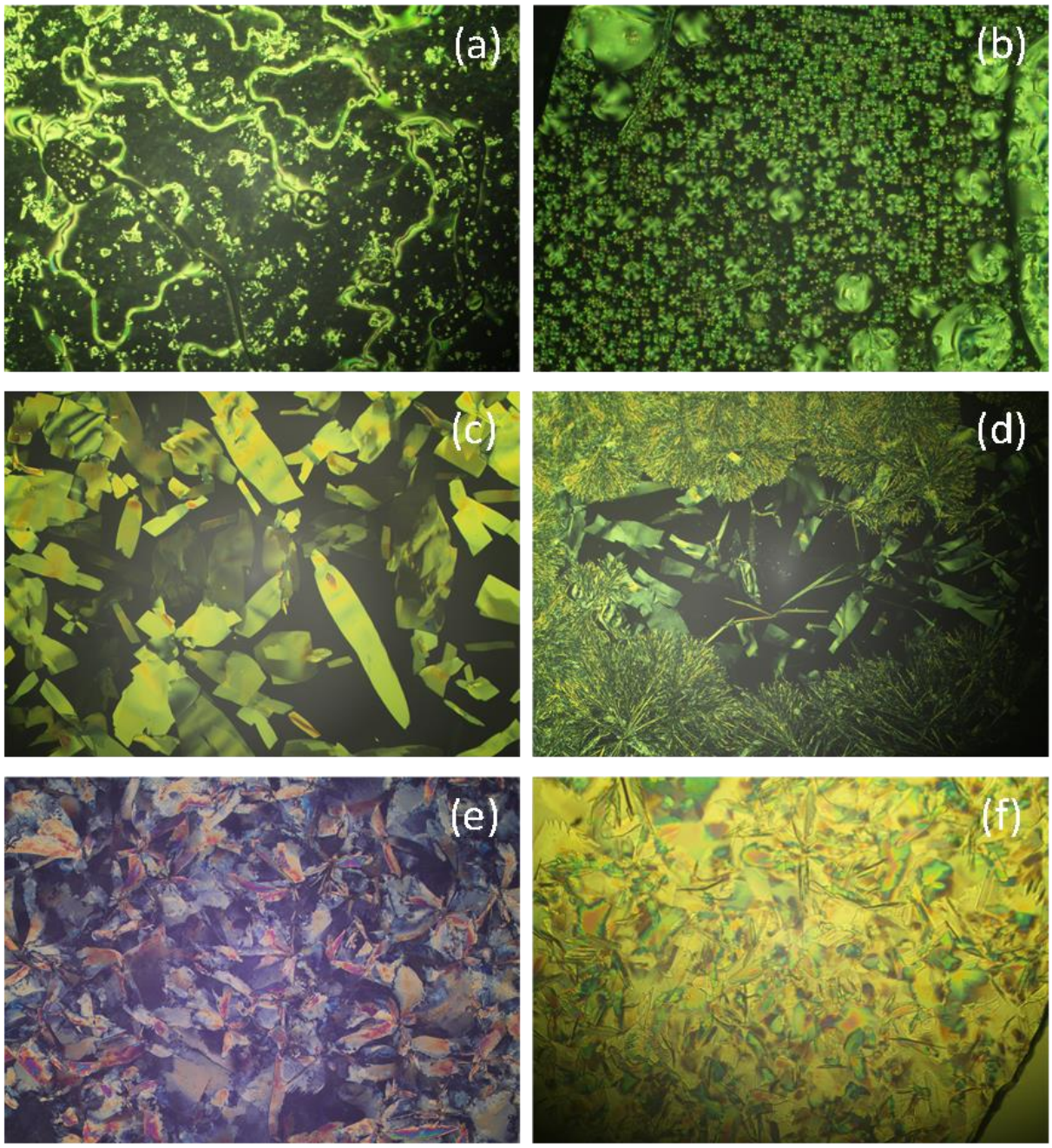

Figure 5.5: Microphotographs of the textures observed under POM for the different LC phases of compounds placed between two untreated glass substrates **(a)** Thread like texture of nematic (N) phase of **8c** at 141°C, **(b)** transition from nematic to smectic A in cooling cycle of **8f** at 156°C, **(c)** batonnet texture of SmA phase mesophase of **8j** at 185°C, **(d)** SmA to Cr transition of **8j** at 104°C, **(e)** monotropic SmC mesophase of **8l** at 135°C, **(f)** monotropic SmC mesophase of **8m** at 116°C

Table 5.1: Phase transition temperature of compounds **8a-m**[a, b]

Sample code	n-alkyl chain	Heating Temp °C [ΔH kJ mol^{-1}]	Cooling Temp °C [ΔH kJ mol^{-1}]
8a	**1**	Cr 119.4 [25.56] N 235.6 [0.55] I	I 234.7 [0.64] N 98.2 [21.27] Cr
8b	**2**	Cr 126.7 [37.76] N 241.6 [1.12] I	I 240.4 [1.07] N 80.6 [32.16] Cr
8c	**3**	Cr 137.2 [29.30] N 232.8 [1.08] I	I 231.2 [0.83] N 106.4 [30.70] Cr
8d	**4**	Cr 149.2 N [24.86] 231.2 [0.78] I	I 229.5 [0.92] N 81.1 [28.04] Cr
8e	**5**	Cr 154.1 [28.88] N 220.3 [0.98] I	I 218.7 [1.17] N [30.18] 74.5 Cr
8f	**6**	Cr 153.8 [43.58] SmA 162.7 [1.08] N 214.5 [0.86] I	I 212.8 [1.47] N 157.4 [0.58] SmA [47.54] 106.3 Cr
8g	**7**	Cr 148.2 [32.03] SmA 169.0 [1.26] N 208.8 [0.74] I	I 205.9 [0.83] N 161.6 [0.91] SmA 102.2 [36.51] Cr
8h	**8**	Cr 143.1 [29.80] SmA 175.5 [0.95] N 198.7 [0.70] I	I 195.5 [1.08] N 168.3 [1.01] SmA 108.2 [32.67] Cr
8i	**10**	Cr 131.2 [24] SmA 182.6 [0.68] N 192.6 [0.54] I	I 190.6 [0.47] N 176.1 [0.60] SmA 98.5 [18] Cr
8j	**12**	Cr 125.5 [48.59] SmA 188.2 [2.30] I	I 187.8 [1.84] SmA 104.8 [52.16] Cr
8k	**14**	Cr 119.0 [39.14] SmA 184.1 [1.45] I	I 183.5 [1.60] SmA 97.6 [41.60] Cr
8l	**16**	Cr 112.5 [40.26] SmA 178.4 [2.03] I	I 178.0 [1.78] SmA (137.6) SmC^{c} 70.8 [45.60] Cr
8m	**18**	Cr 108.3 [31.42] SmA 170.9 [1.89] I	I 170.2 [1.241] SmA (118.0) SmC^{c} 76.1 [39.13] Cr

Temperature in parenthesis ( ) indicates monotropic transition; Cr = crystal, Sm = smectic phase, N = nematic phase, I = isotropic.

[a]Phase transition temperatures were determined/confirmed by both polarizing optical microscope (POM) and differential scanning calorimetry (DSC) studies: peak temperatures in the DSC

thermograms obtained during the first heating and cooling cycles (scanning rate = 5°C min^{-1}) coupled with POM measured temperatures are given; [b]Transition temperatures of some of the compounds were determined with the aid of a POM study as the expected well-resolved thermograms of both heating and cooling cycles could not be obtained; [c]Phase transition was observed under POM; enthalpy change too weak to be detected by DSC.

5.3.3. Thermal properties

The phase transition temperatures, enthalpy changes, and mesophase textures of the various compounds **(8a–m)** are briefly described in **Table 5.1**. The combination of DSC studies **(Figure 5.6 (a)** and **(b))** and observations utilizing POM resulted in distinguished transition temperatures and textures for all the compounds in the series. These findings were consistent with each other over many heating and cooling cycles. Compounds **8a-e** exhibited a total of four peaks, two of which were endothermic and two were exothermic, in both the heating and cooling cycles. Among these peaks, one shown a very low enthalpy change. The peak exhibiting a low enthalpy change corresponds to the N*-Iso transition. This peak reflects comparatively weak molecular interactions that exist in the nematic phase, which requires a lesser amount of energy to be disrupted as the system transitions into the isotropic phase. On the other hand, the peak displaying a higher enthalpy change can be attributed to the Cr-N and N-Cr phase transition. Three endothermic peaks and three exothermic peaks are observed in the heating and cooling cycles, respectively, for compounds **8f-i**. In the heating cycle, the Cr-N transition is associated with the first peak with a high ΔH value, followed by the N-SmA and SmA-Iso transitions with two subsequent peaks. In the cooling cycle, the three exotherms indicates the transitions between Iso-SmA, Sm-N, and N-Cr. There are two exothermic peaks and two endothermic peaks for compound **8j-m**. Two peaks during the heating cycle correspond to the Cr-SmA and SmA-Iso transitions, which were also apparent during the cooling cycle as the Iso-SmA and SmA-Cr transitions, respectively. Furthermore, a cooling cycle for compounds **8l** and **8m** utilizing POM revealed the presence of SmC mesophase; however, the phase was not detectable on DSC thermograms. Compared to other phase transitions, SmA-SmC is frequently distinguished by a transition that is comparatively weak, as it primarily involves a modification in molecular ordering without a substantial shift in molecular packing density. Consequently, it is possible that the transition doesn't involve a considerable enthalpic changes, which would generate a distinct peak on the DSC thermogram.

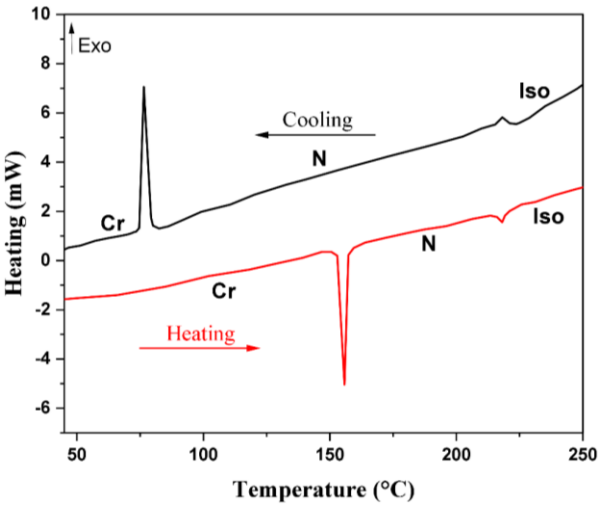

Figure 5.6 (a): DSC thermogram of **8e**

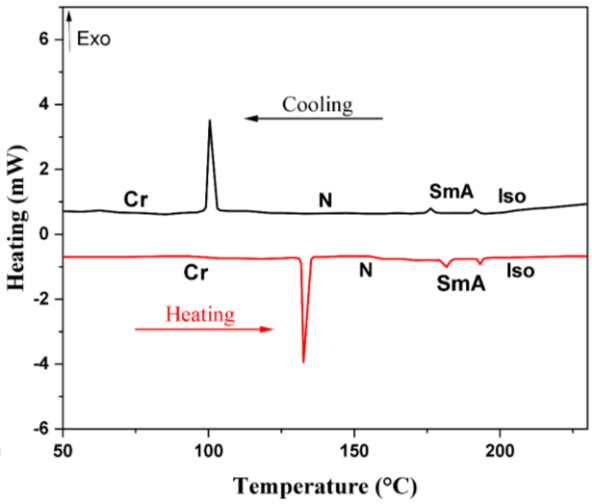

Figure 5.6 (b): DSC thermogram of **8i**

All compounds in **Table 5.1** have very predictable enthalpy changes following the initially occurring transition of crystal-nematic/smectic A. However, the nematic-isotropic transition has fewer enthalpy changes than expected. Again, this behaviour is expected from typical mesogens like this.

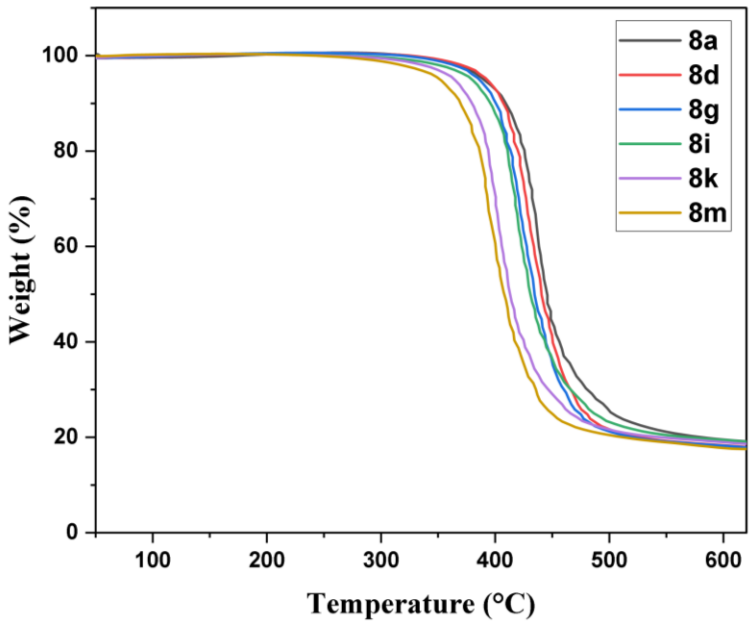

Figure 5.7: TGA profile for some of the oxadiazole derivatives

In order to evaluate the thermal stability of compounds **8a**, **8d**, **8g**, **8i**, **8k** and **8m**, thermogravimetric analysis (TGA) was used.

All oxadiazole derivatives were found to be stable within a temperature range of 314 to 558°C, the initial degradation temperature (IDT), 50% decomposition temperature, and the final decomposition temperature (FDT) for each respective derivative are provided in **Table 5.2**. In particular, the compounds exhibit LC property prior to undergoing thermal

decomposition. Compound **8d** had the greatest initial thermal decomposition temperature, which was 355°C, whereas compound **8m** displayed the lowest IDT, which was 314°C. The observations presented here suggest that there is a lower probability of thermal decomposition occurring within this temperature range, as shown in **Figure 5.7** respectively. In addition, the decomposition process was completed within the range of 499 to 557°C, and the 50% decomposition of all of the derivatives that were investigated took place within the temperature range of 407 to 444°C.

Table 5.2: TGA thermograms decomposition temperatures for compounds **8a, 8d, 8g, 8i, 8k** and **8m**

Sample Code	IDT (°C)	50% DT (°C)	FDT (°C)
8a	353	444	557
8d	355	440	542
8g	346	434	513
8i	334	430	512
8k	328	412	505
8m	314	407	499

IDT = initial degradation temperature, 50% DT = 50 % decomposition temperature, FDT = final decomposition temperature

5.3.4. Structure-mesomorphic property relationship

Figure 5.8 shows a graph demonstrating the correlation between the transition temperature and the total number (n) of C-atoms in the alkoxy chain. The diagram provides information on many transition curves, including solid-mesophase, SmA-N, SmA-SmC and N/SmA-Iso.

The transition temperatures from the N*/SmA phase to the isotropic phase have been represented on a single curve. The initial members of the series on this curve exhibit a noticeable odd-even effect. The phase transition throughout SmA to N* shows a consistently rising curve, reaching the peak at the decyloxy derivative. The SmA to SmC phase transitionn (observed only on cooling/monotropic), show a rising tendency. The curve representing phase transition from solid to intial mesophase keep rising until the pentyloxy derivative where an increasing terminal chain length hinders the parallel arrangement of molecules, leading to a narrower liquid crystalline mesophase range. Subsequently, a sharpe decline is observed upon entering the smectic mesophase (from hexyloxy onwards) which follows the declining trend

till the octadecyl derivative. In general, the mesogenic properties were largely impacted by the length of the alkoxy chain. With an increase in the number of carbon chains, both melting and clearing temperatures decreased. Enhanced flexibility of the molecule contributed to a decrease in terminal attraction, resulting in reduced phase stability [49]. The emergence of the Smectic phase from middle homologues in this types of system is frequently observed [50,51]. In lower homologues, the aromatic nuclei are minimally separated, leading to intense terminal interactions and the occurrence of exclusively nematogens. As we proceed in the series, an increase in terminal chain length strengthens the lateral cohesive forces, leading molecules to arrange in a layered structure before moving into the nematic phase. As the methylene units in the chain increases, the smectogenic characteristic is projected to become more dominant over the constancy of N mesophase due to weak terminal intermolecular interactions being inadequate to sustain parallel molecular orientation.

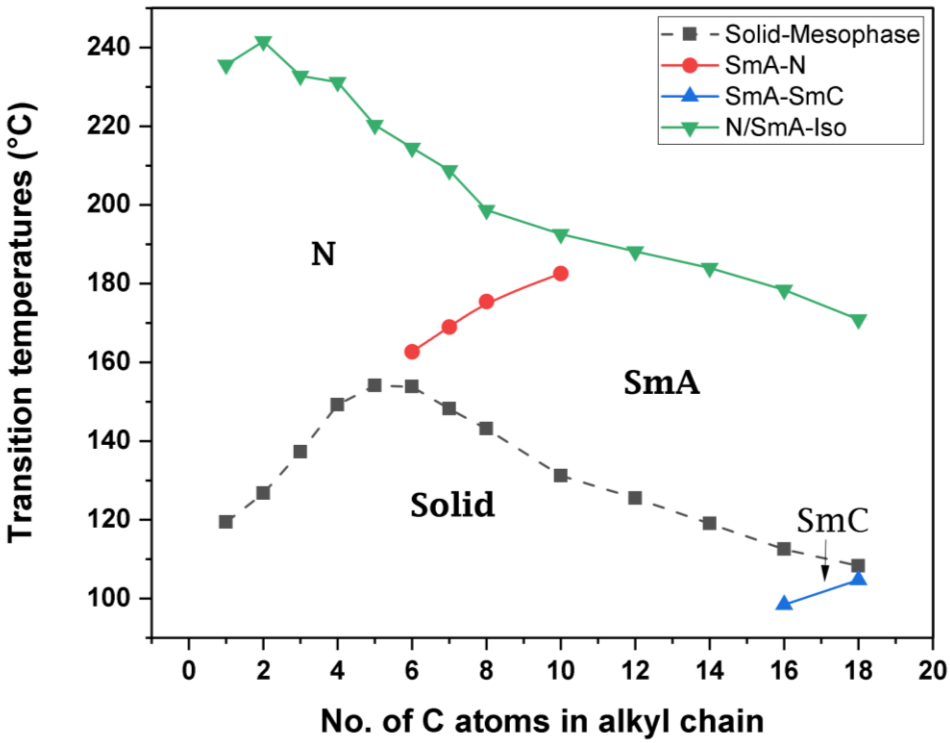

Figure 5.8: Plot of transition temperatures (°C) versus number of carbon atoms in the alkoxy chain

The molecular structure of organic compounds influences their LC properties, which in turn affect their thermal stability. By analysing the molecular composition, we can establish a correlation between the mesogenic properties and thermal stability of these derivatives, particularly in terms of isotropic points and the stability of different phases. **Table 5.3** presents a comparative analysis of the average thermal stabilities across various LC series.

Comparison of molecular structure of present **Series I** with reported series:

(1) 5-(4-n-alkoxy phenyl)-2-(4-(4′-methoxy benzoyloxy)) benzylideneamino-1,3,4-oxadiazoles; **Series I**

(2) "5-(4-n-Decyloxy)-phenyl-2-[4-(4′-n-alkoxy-benzoyloxy)-3-methoxy]-benzylidene-amino-1,3,4-thiadiazoles"; **Series A** [52]

(3) "4-(5-(4-Nitrophenyl)-1,3,4-oxadiazol-2-yl) phenyl-4-((4-alkoxybenzylidene) amino) benzoate"; **Series B** [53]

(4) "5-(4-n-Decyloxy)-phenyl-2-(2-hydroxy-4-n-alkoxy)-benzylideneamino-1,3,4-oxadiazoles"; **Series C** [54]

The geometry of the series is given in **Figure 5.9**.

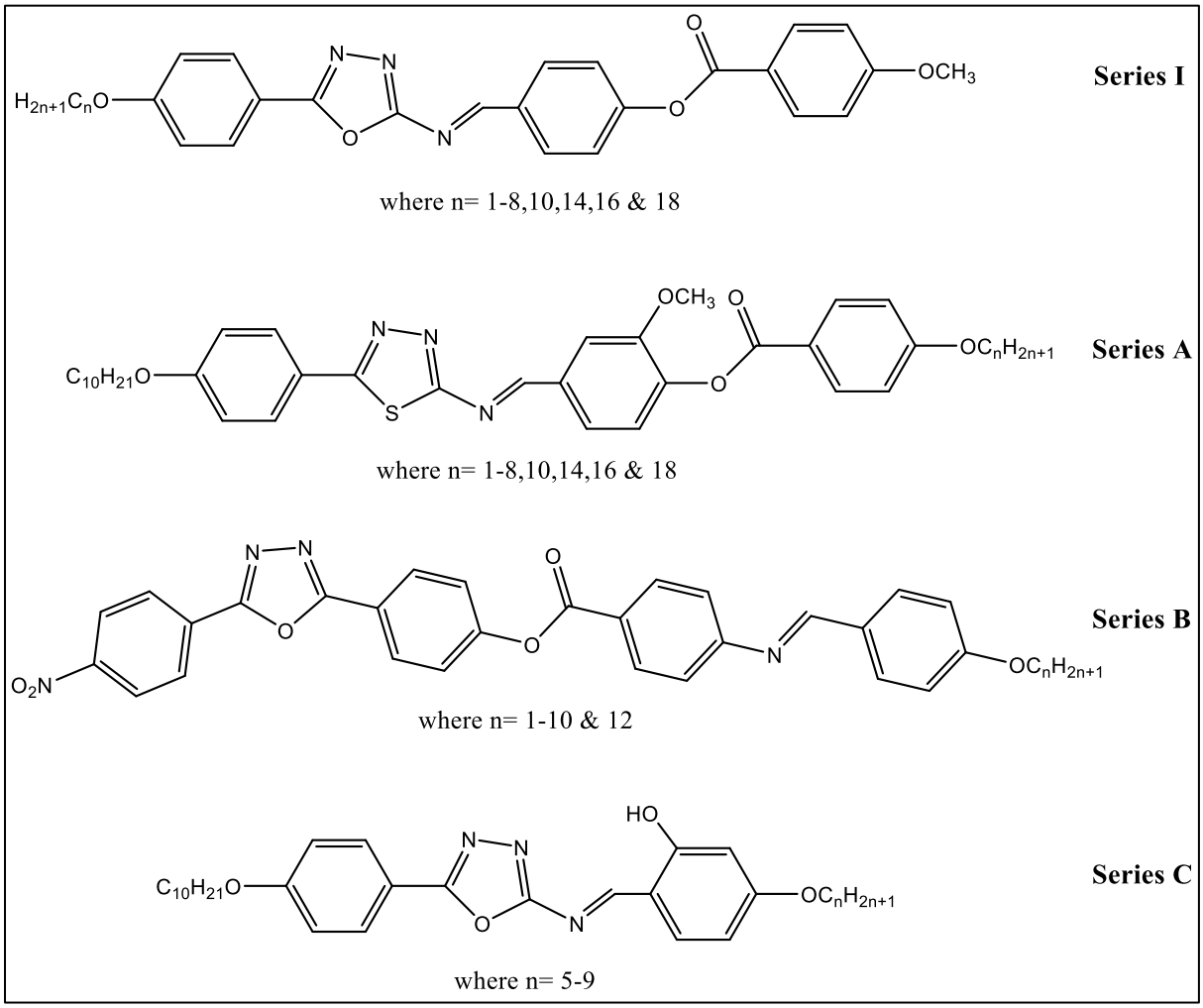

Figure 5.9: The geometric comparison of **Series I, A, B** and **C**

In compounds from Series I, the 5-(4'-n-alkoxy phenyl)-2-amino-1,3,4-oxadiazoles are linked to the 4-(4′-methoxybenzoyloxy) benzaldehyde to give the final Schiff's base derivatives, while in Series A, the 5-(4′-n-decyloxy)-phenyl-2-amino-1,3,4-thiadiazole is

linked to various 4-(4′-n-alkoxybenzoyloxy)-3-methoxybenzaldehydes to form the final Schiff's bases with lateral methoxy substitution. As reported in the literatures [55–57], generally it was seen that the thidiazole based liquid crystals showed higher thermal and mesophase stability compared to the analogous oxadiazole derivatives. Here, from the **Table 5.3,** it was observed that Series I and A had very similar N-Iso range. As explained by Gray [58] this may be accredited to the existence of lateral -OCH_3 substitution which increases the breadth of the molecules thus increasing the length to breath ratio and polarizability which can increase intermolecular attractions between the molecules resulting into the reduced clearing temperature and mesophase stability. The current investigation aligns with Gray's perspective, providing further support for his viewpoint.

Table 5.3: Average thermal stabilities (°C) of Series I, A and B compounds.

Series	**I**	**A**	**B**	**C**
N - Iso	219.5 ($C_{1\text{-}8,10}$)	216.8 ($C_{1\text{-}8,10}$)	260.8 ($C_{1\text{-}10}$)	-
SmA/SmC - N	172.4 ($C_{6\text{-}8,10}$)	154.0 ($C_{7,8,10}$)	217.6 ($C_{6\text{-}10}$)	-
Commencement of Smectic phase	Hexyloxy	Heptyloxy	Pentyloxy	-

In Series B, the oxadiazole is linked to p-nitro phenyl on 5 position and reversed azomethine and ester group with an additional phenyl ring. As given in **Table 5.3,** the Series B shows high thermal stability than Series I this may be due to the presence of nitro (-NO_2) terminal group. The nitro group's high electronegativity and polarity, resulting in stronger intermolecular forces, such as dipole-dipole interactions and hydrogen bonding. These interactions lead to increased molecular cohesion and thus the higher thermal stability of Series B.

In Series C, the amino oxadiazole moiety is linked to 2-hydroxy-4-n-alkoxy-benzaldehyde. This compound was found to be non-mesogenic, which may be due to the absence of a linking groups in the other part of the molecule. Linking groups ensures basic linearity and structural compatibility. By increasing the extent and polarizability anisotropy of the fundamental unit, these compounds improve mesophase stability and melting point, resulting in larger mesophase range as observed for Series I.

Thus, from the above discussions it can be concluded that even small alteration into the molecular structure results into substantial change into the liquid crystalline properties of the molecule.

5.3.5. Radical-scavenging activity of mesogens

Studies have demonstrated that substituted 1,3,4-oxadiazole scaffolds exhibit diverse biological properties. Specifically, research suggests that 2,5-disubstituted 1,3,4-oxadiazole derivatives, commonly synthesized from diacylhydrazines or semicarbazones, possess antioxidant activities [59–61].

Table 5.4: Radical-scavenging activity of mesogens: % inhibition and IC_{50} values of the DPPH free radical scavenging assay

Sample code	% Inhibition[a]			IC_{50} (µg/ml)
	50 µg/ml	100 µg/ml	200 µg/ml	
8a	46.08 ± 0.30	65.98 ± 0.32	88.87 ± 0.73	55.43
8b	44.68 ± 0.95	66.48 ± 0.58	85.04 ± 0.75	56.79
8c	44.56 ± 0.66	62.16 ± 0.09	83.06 ± 0.61	63.58
8d	40.35 ± 0.21	59.36 ± 0.66	80.48 ±0.03	77.88
8e	39.16 ± 0.45	56.9 ± 0.51	77.34 ± 0.42	85.12
8f	39.38 ± 0.94	57.11 ± 0.26	78.2 ± 0.86	83.98
8g	36.87 ± 0.31	54.26 ± 0.06	75.6 ± 0.92	94.51
8h	34.6 ± 0.76	51.63 ± 0.41	70.55 ± 0.62	106.92
8i	33.21 ± 0.33	52.04 ± 0.29	66.76 ± 0.02	113.54
8j	30.28 ± 0.86	49.82 ± 0.90	63.96 ± 0.20	125.95
8k	30.75 ± 0.20	44.69 ± 0.28	61.1 ± 0.86	139.43
8l	31.42 ± 0.26	41.43 ± 0.69	58.88 ± 0.22	150.24
8m	29.26 ± 0.16	42.08 ± 0.90	56.64 ± 0.08	158.03
STD[b]	48.84 ± 0.35	63.33 ± 0.03	90.64 ± 0.32	53.31
Blank[c]	-	-	-	-

[a] Values represent the mean ± standard error mean (SEM) of three experiments.

[b] Ascorbic acid used as standard

[c] No inhibition

All the synthesized mesogens were tested for their radical scavenging activity (anti-oxidant activity) using the DPPH free radical assay and method described in the literature [62].

0.01 mg/mL (0.001% (w/v)) solution of DPPH in methanol was prepared and mixed with an equal amount of standard antioxidant and synthesized 1,3,4-oxadiazoles dissolved in methanol. Stock solutions of synthesized compounds (1 mg/mL) was diluted to a final concentration of 50, 100, and 200 µg/mL in DMSO. The absorbance was recorded at 517 nm using a Shimadzu UV-1800 spectrophotometer from Japan after a 30-minute incubation in darkness. The DPPH radical scavenging activity of synthesized compounds has been compared to the well-known reference antioxidant, ascorbic acid. DPPH radical scavenging activity was determined as:

$$\text{“\% Inhibition} = [(A_{control} - A_{sample}) / A_{control}] \times 100\text{”}$$

where $A_{control}$ = absorbance of the control, A_{sample} = absorbance of the test compounds.

Results are represented as a percentage of inhibition and an IC_{50} value, which represents the effective concentration needed to scavenge 50% of the original DPPH. It was compared to the referent ascorbic acid.

Results from the **Table 5.4** indicate that all of the compounds possess moderate to good radical scavenging activity. Notably, the lower homologues displayed comparatively better activity than the analogous higher homologues. The highest activity with an IC_{50} value of 55.43 µg/ml was observed for compound **8a**, and compound **8m** showed the lowest activity with an IC_{50} value of 158.03 µg/ml among all. The higher activity in the lower homologues compared to the higher homologues can be attributed to the smaller molecular size and higher solubility of the compounds.

5.3.6. Optical Properties

The UV-visible absorption spectra of the oxadiazole derivatives **8a-m** were measured using $CHCl_3$ as the solvent. The UV spectra for all compounds are depicted in the **Figure 5.10**. As shown in the **Table 5.5**, all compounds exhibit similar absorption peaks, owing to their structural resemblance. The maximum absorption wavelength (λ_{max}) for all compounds is approximately 324 nm. In the absorption spectra, the higher-energy band at around 254 nm arises from π-π* electronic transitions of the phenyl ring, while the lower-energy band at approximately 324 nm is attributed to the n-π* transition of the azomethine linkage (CH=N). Interestingly, variations in chain length did not significantly influence the optical properties. Compound **8h** exhibited the highest absorbance, while compound **8k** displayed the lowest absorbance.

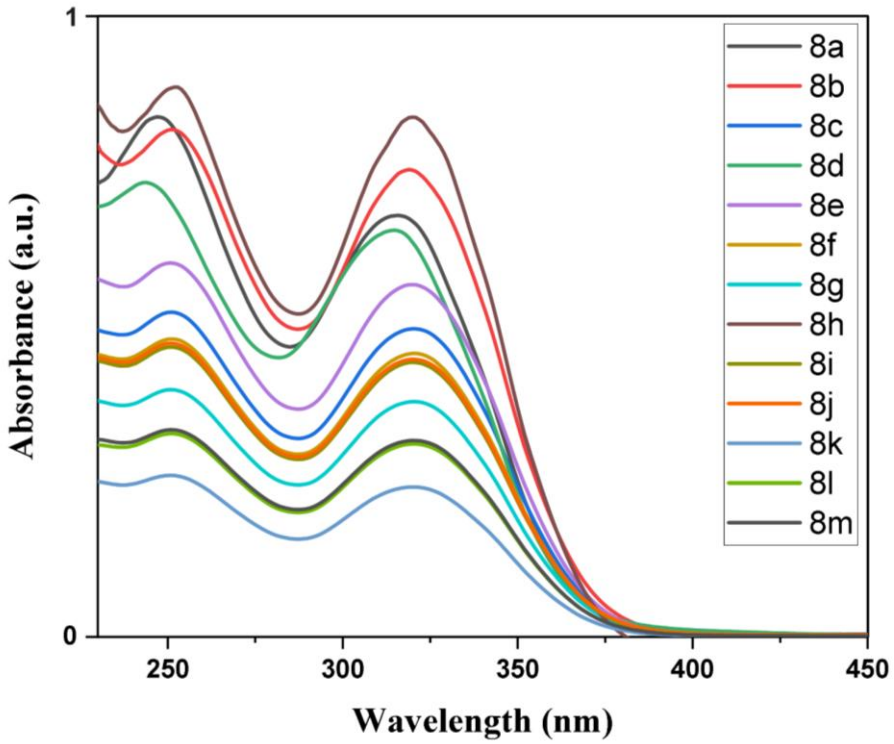

Figure 5.10: UV absorbance spectra of compounds **8a-m**

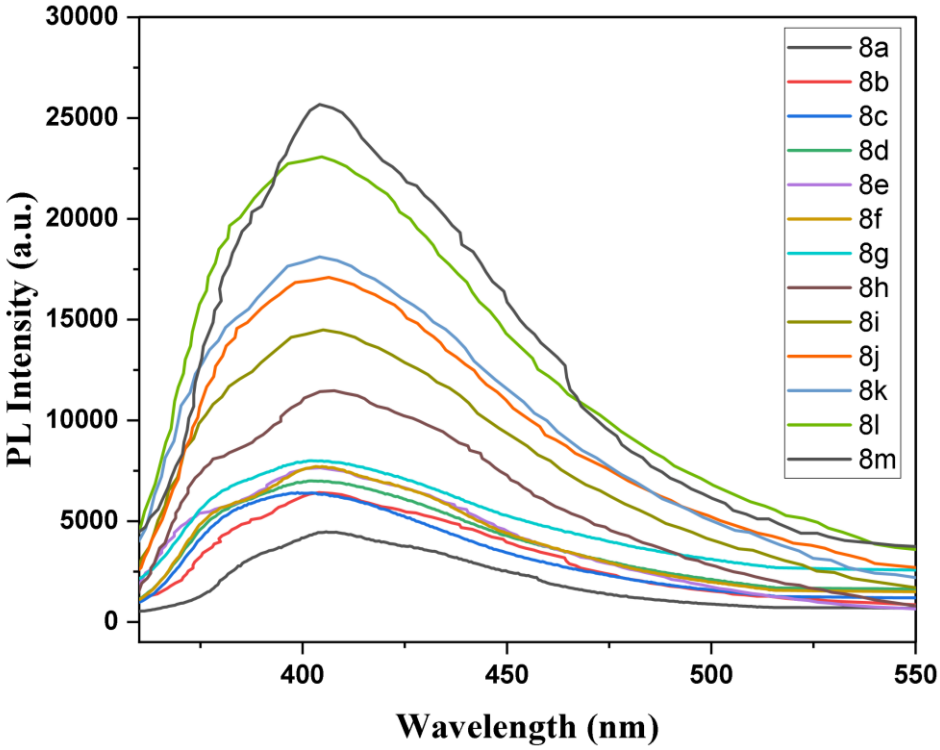

Figure 5.11: Fluorescence spectra of compounds **8a-m** in chloroform ($1x10^{-5}$M). All of the compound were excited at 325 nm

The photoluminescence spectra of compounds **8a-m** were recorded in $CHCl_3$ solvent (1×10^{-5} M) across the range of 300 to 800 nm, with an excitation wavelength of 325 nm, to investigate the relationship between photophysical properties and molecular structure. Both excitation and emission bandwidths were maintained at 5 nm during the analysis. Notably, all compounds **8a-m** displayed intense fluorescence at approximately 405 nm, falling within the blue emission region spanning from 390 to 450 nm **(Figure 5.11)**. Details of the photophysical data for each compound are provided in the accompanying **Table 5.5**. Interestingly, an increase in the terminal chain length resulted in a consistent enhancement in fluorescence intensity. Assessment of fluorescence quantum yields in $CHCl_3$ solution revealed remarkable values ranging between 0.35 to 0.59 for all compounds, in comparison to the standard (quinine sulphate dissolved in 1 N sulphuric acid; Φ_{PL} = 0.546), indicating their strong fluorescence efficiency. Moreover, higher homologues within the series exhibited stronger emissions, leading to higher fluorescence quantum yields. The stokes shifts observed for all compounds were nearly identical, ranging from 78 to 85 nm.

Table 5.5: UV and fluorescence peaks for compounds **8a-m.**

Compounds	UV (nm)	Fluorescence(nm)	Stokes shift(nm)[a]	Φ_{PL}[b]
8a	253, 320	405	85	0.35
8b	255, 322	404	82	0.38
8c	254, 323	401	78	0.38
8d	247, 319	402	83	0.41
8e	254, 323	403	80	0.45
8f	254, 324	403	79	0.45
8g	254, 323	401	78	0.47
8h	256, 324	405	81	0.49
8i	254, 323	405	82	0.51
8j	254, 324	406	82	0.55
8k	254, 323	404	81	0.55
8l	255, 324	404	80	0.58
8m	254, 324	404	80	0.59

[a]Excited at 325 nm

[b]Determined using quinine sulphate as standard (Φ_{PL} = 0.546 in 1N H_2SO_4)

In summary, the synthesized compounds exhibit photoluminescence spectra with emissions in the blue region (400–470 nm), suggesting their suitability for various applications.

These materials possess blue light emission properties, making them potentially valuable for applications such as OLED materials, biotags for biological sensing and fluorescent probes in biological applications.

5.3.7. DFT studies

5.3.7.1. Optimized Molecular Structures and HOMO-LUMO energies

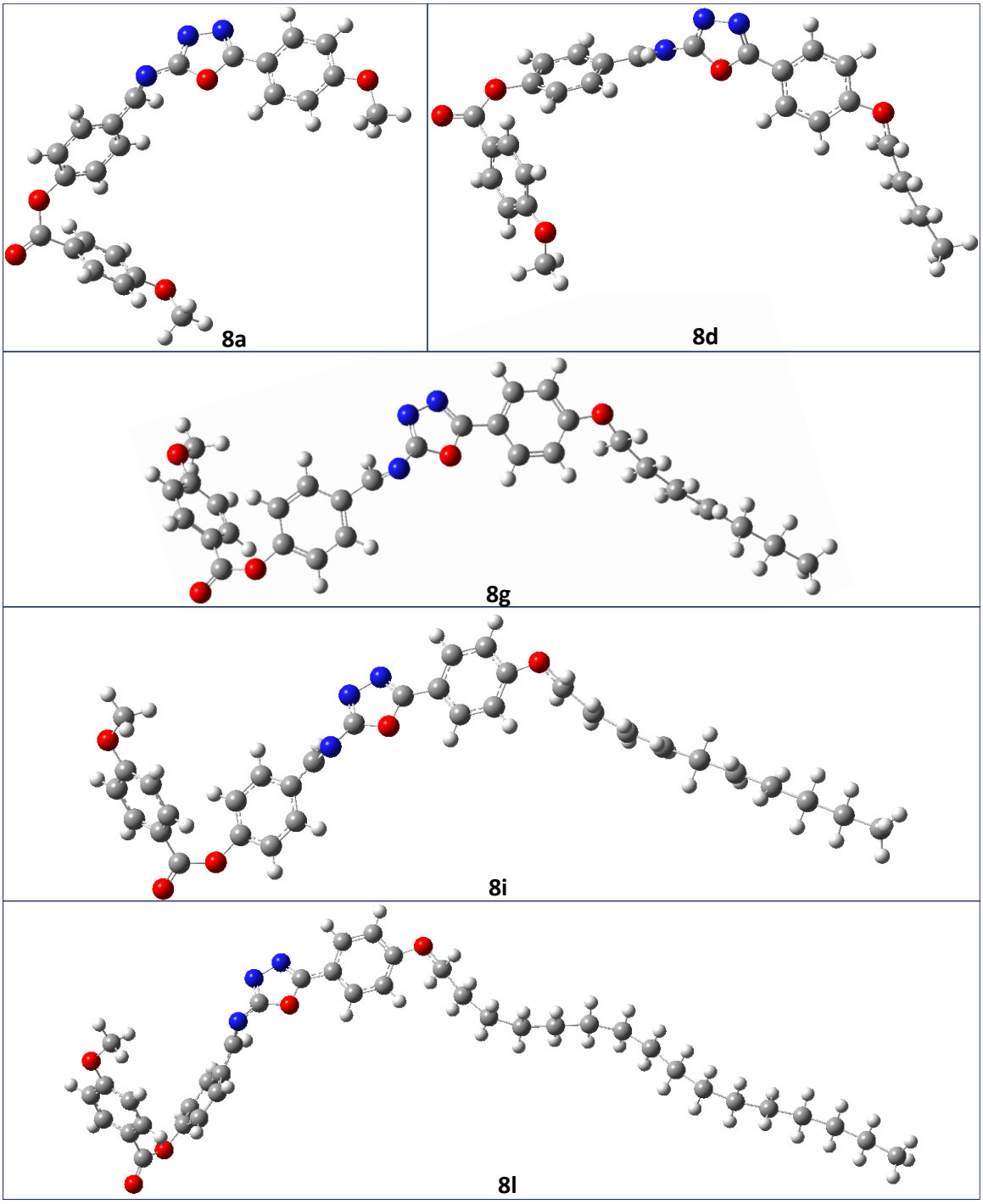

Figure 5.12: Optimized molecular structures of thiadiazole cholesterol derivatives

DFT analysis was employed to investigate the molecular conformation, molecular orbitals, and electrostatic potential of oxadiazole derivatives. Geometry optimizations and DFT calculations were performed using Gaussian 09, revision A.02 with B3LYP hybrid functional and 6-31G (d, p) basis set [63]. The absence of any imaginary frequency in the optimized structure confirms its stable energy state **(Figure 5.12)**. **(Figure 5.12)** depicts the optimized molecular configuration observed for oxadiazole derivatives. **Table 5.6** provides the optimized energies for specific derivatives, while **Figure 5.13** illustrates the relationship between the number of carbon atoms in the terminal chain of synthesized compounds and the energy minima in Hartree units. The graph reveals a decrease in energy minima with an increase in the number of carbon atoms in the terminal chain, suggesting greater stability in the molecular structure. This implies that longer chains may lead to more favorable conformations energetically, possibly due to enhanced flexibility and conformational freedom within the molecule.

The HOMO and LUMO are essential in assessing a compound's stability, reactivity, and light absorption. A wider HOMO-LUMO energy gap indicates increased stability and reduced reactivity, as the compound is less likely to accept or donate electrons. HOMO acts as an electron donor, while LUMO functions as an electron acceptor. **Table 5.7** presents the calculated values of the frontier molecular orbital energies and the HOMO-LUMO energy gap for oxadiazole molecule and 3D iso-surface maps of these orbitals for the compounds can be found in **Figure 5.14 (a-b)**.

Table 5.6: Optimized energy (in Hartree)

Sample	Energy Minima (Hartree)
8a	-1465.699
8d	-1582.966
8g	-1700.258
8i	-1817.519
8l	-2052.163

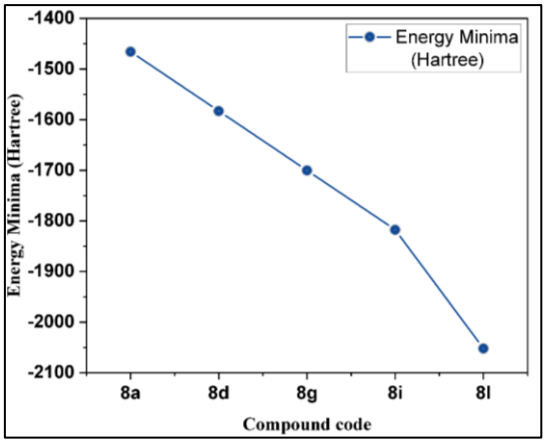

Figure 5.13: Dependence of the terminal alkoxy chain on the energy minima.

Table 5.7: Calculated molecular properties of the oxadiazole compounds using DFT

Sample	E_{HOMO} (eV)	E_{LUMO} (eV)	ΔE (eV)	η Global hardness	$\delta = 1/\eta$ Global softness	μ_{el} (eV)	ω Electro-philicity index
8a	-5.918	-2.0166	3.90	1.95	0.51	-3.96	4.03
8d	-4.349	-2.299	2.04	1.02	0.97	-3.32	5.39
8g	-3.182	-2.116	1.06	0.53	1.87	-2.64	6.58
8i	-2.865	-2.004	0.86	0.43	2.32	-2.43	6.89
8l	-2.994	-2.283	0.71	0.35	2.81	-2.63	9.79

The electron density of the orbitals in the HOMO in all the compounds was mostly concentrated over the alkoxy terminal chain of the oxadiazole moiety, except of **8a** where it was mainly focused over the oxadiazole moiety, aromatic ring, azomethine and methoxy group.

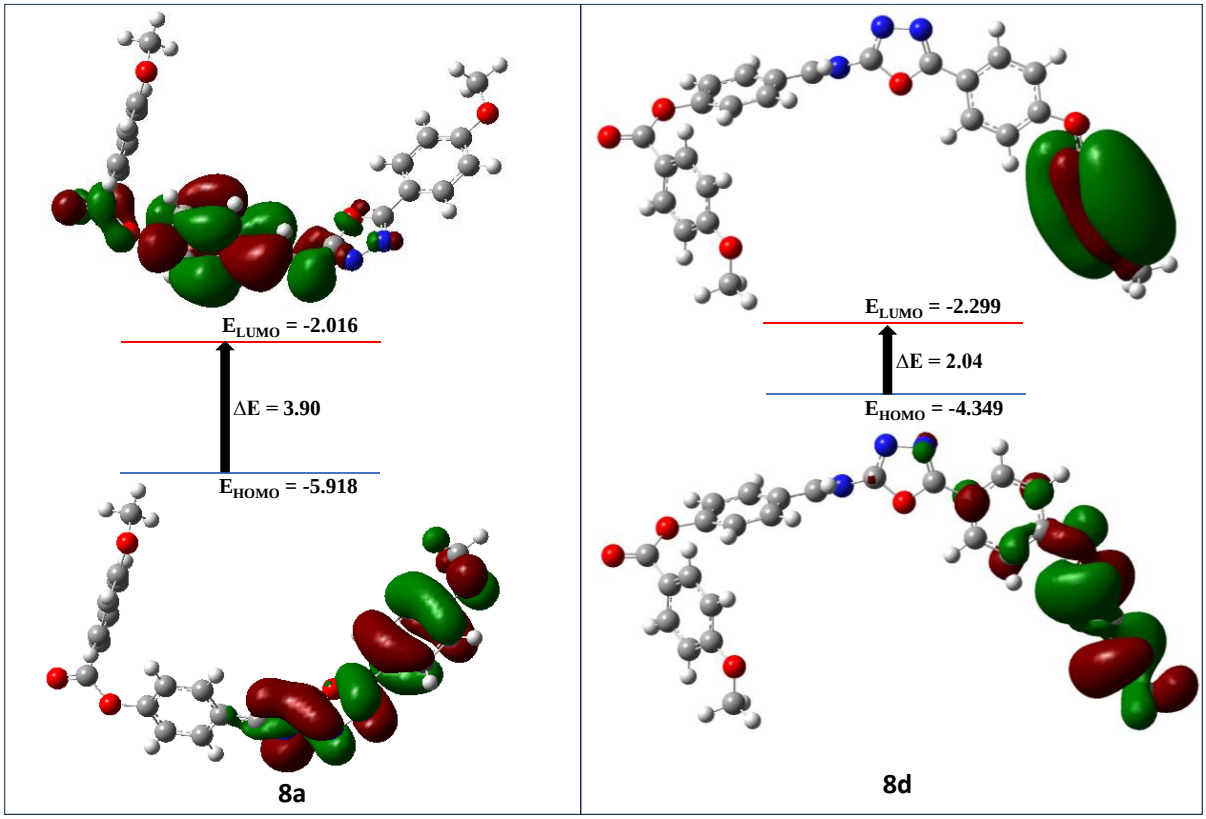

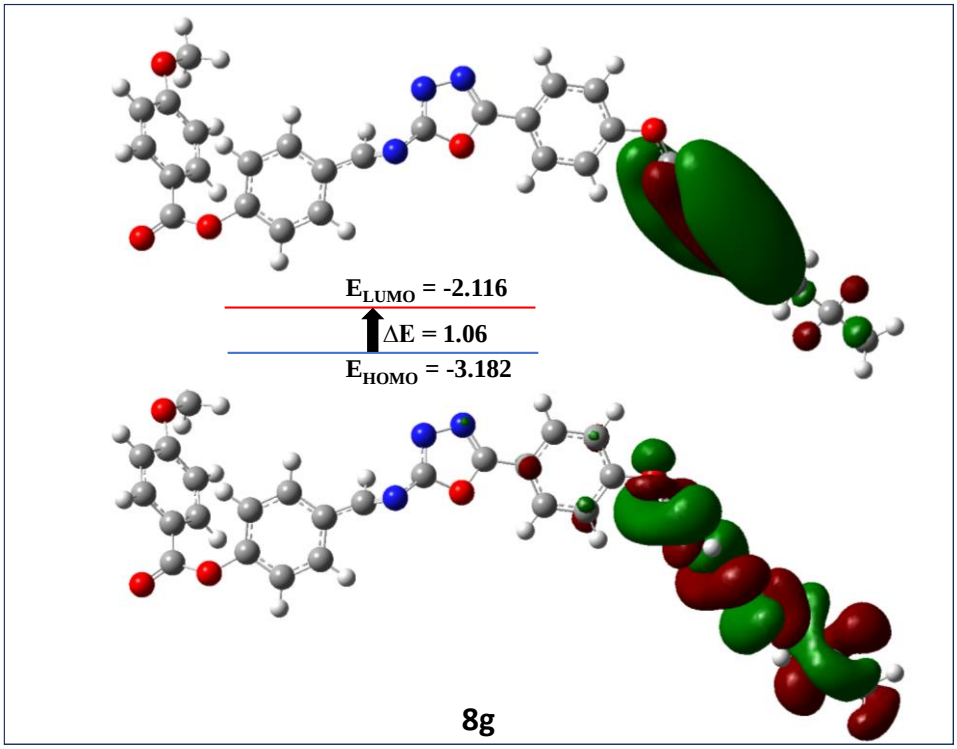

Figure 5.14 (a): FMO contours of structures **8a, 8d** and **8g**

Also, the electron density of the orbitals in the LUMO was mainly concentrated over the terminal alkoxy chains. Electron density for LUMO in **8a** was observed on the aromatic part of the molecule, azomethine and ester linkage. The energy gap (ΔE) for synthesized oxadiazole compounds were found to be in the range of 3.90 – 0.71 with decreasing trend for increased methylene units. This implies that the lower homologues in the series exhibit greater stability and lower reactivity, while increasing the terminal chains enhances the likelihood of the molecule engaging in electronic transitions and chemical reactions. This suggests heightened reactivity of the molecule, potentially leading to improved electrical conductivity or fluorescence characteristics.

Table 5.7 presents the frontier Molecular Orbital (MO) energy levels and various reactivity parameters for optimized molecular structures [64], providing significant insights into the chemical reactivity and stability of the compounds. The compounds displayed chemical potentials ranging from -2.43 to -3.96 eV and hardness values ranging from 0.35 to 1.95 eV, with the lowest observed for compound **8l**. Compound **8l** exhibits higher reactivity compared to others in the series, indicating its softer nature. Furthermore, a trend of increasing electrophilicity is noted in the sequence: **8a** < **8d** < **8g** < **8i** < **8l**, suggesting a decrease in electron density or an increase in electron-withdrawing characteristics among the mesogens. Consequently, **8l** displays enhanced reactivity towards electrophiles.

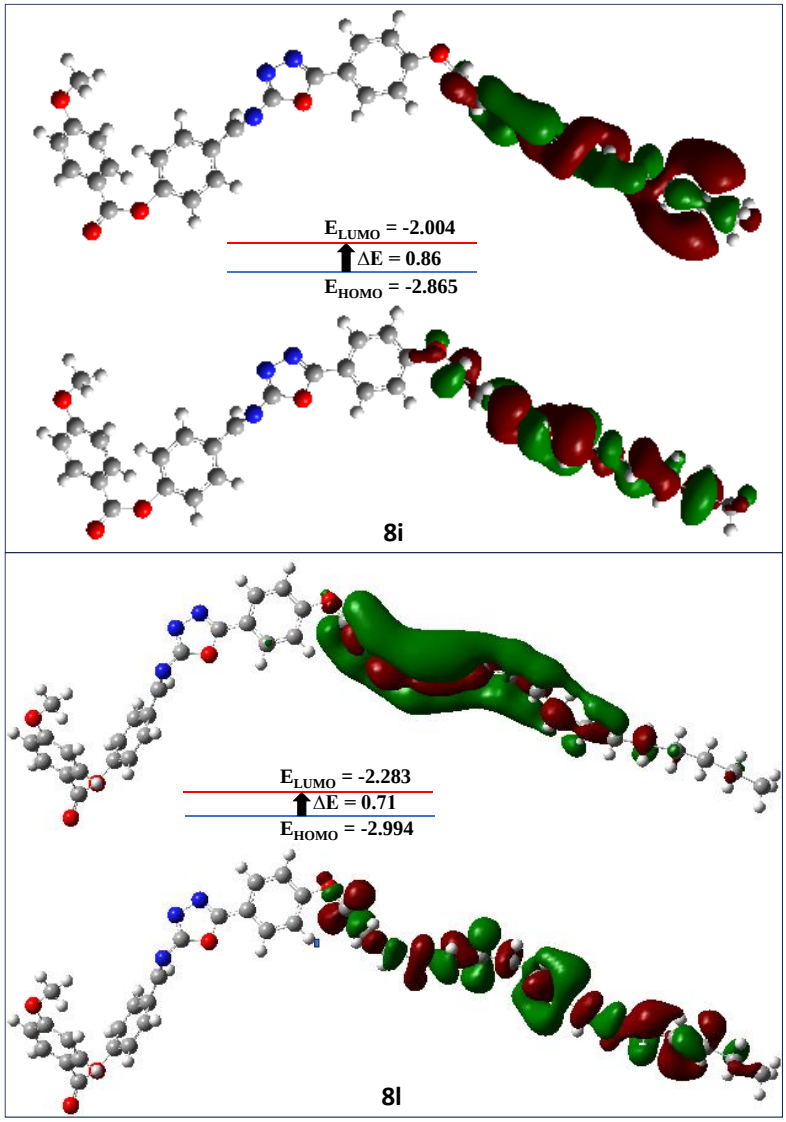

Figure 5.14 (b): FMO contours of structures **8i** and **8l**

Table 5.8: Dipole moment for oxadiazole derivatives

Sample	μ_x	μ_y	μ_z	Dipole Moment μ_{dip} (Debye)
8a	-0.9634	8.3046	-2.5849	8.7508
8d	3.7262	10.3996	2.2616	11.2761
8g	9.4326	4.4261	4.6425	11.4069
8i	-13.0292	2.3426	2.0554	13.3968
8l	13.6348	-4.7868	2.4759	14.6613

Dipole moments have been computationally determined for the selected compounds along three Cartesian axes **(Table 5.8)**. The elevated dipole moments serve as indicators of the mesogenic characteristics of these compounds. Differences in molecular polarity among the

samples are reflected in their varying dipole moments. Compounds with heightened dipole moments, such as **8i** and **8l**, are anticipated to possess more polarized molecules, while those with lower dipole moments, like **8a** are relatively less polar. These discrepancies in dipole moments play a crucial role in dictating the liquid crystal behaviour, influencing aspects such as phase transitions and optical properties. Elevated dipole moments may potentially amplify electro-optical responses or alter phase transition temperatures.

5.3.7.2. Molecular electrostatic potential (MEP)

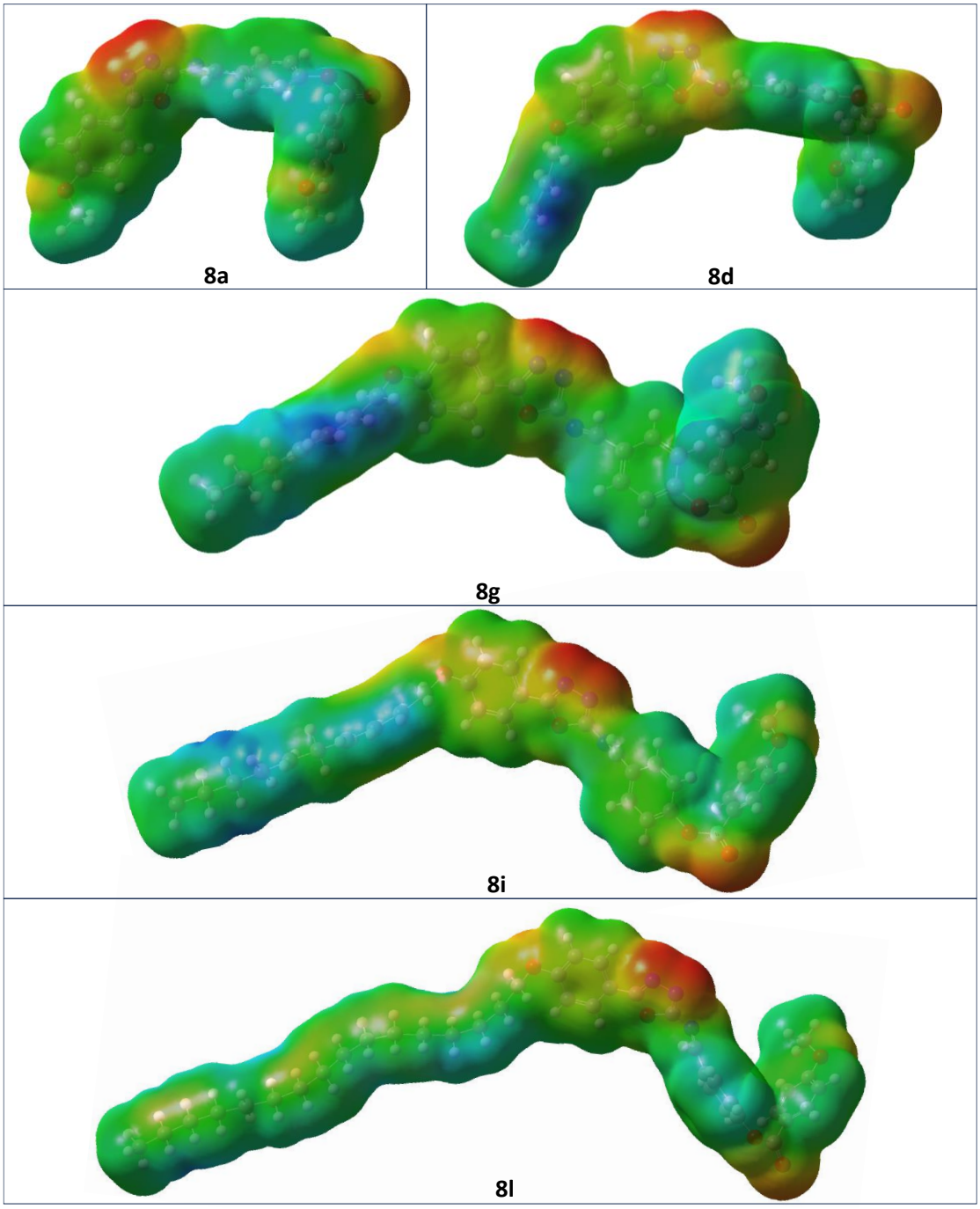

Figure 5.15: MEP mapping of some oxadiazole derivatives

In liquid crystal research, Molecular Electrostatic Potential (MEP) analysis plays a crucial role in understanding the behaviour and properties of liquid crystal molecules. MEP analysis provides insights into the distribution of electric charge within the molecules, which is vital for predicting their interactions, alignment, and overall stability in liquid crystalline phases. Specifically, MEP analysis helps researchers identify regions of high and low electron density within the molecules, which directly influences their response to external electric fields and their ability to form ordered structures.

Figure 5.15 displays the molecular electrostatic potential map, providing valuable insights into intermolecular interactions. In the visualization, the interaction between the electron-rich region (depicted in red) and the electron-deficient region (depicted in blue) signifies intermolecular interactions. The red areas signify regions abundant in electrons, primarily concentrated around the N-N atoms of the oxadiazole ring and ester linkage, indicating negatively charged atomic sites. Conversely, the blue regions represent areas with fewer electrons, with the lowest negative charge observed at the terminal alkoxy chains.

5.4. Conclusion

In summary, thirteen novel liquid crystalline compounds were synthesized through the condensation of 5-(4'-n-alkoxy phenyl)-2-amino-1,3,4-oxadiazole with 4-n-methoxybenzoyloxy benzaldehydes. All compounds 8a-m exhibited mesomorphism. The methyl to n-pentyl homologues demonstrated an enantiotropic N mesophase, whereas the n-hexyl to n-decyl derivatives showed an enantiotropic SmA-N-Isotropic transition. Additionally, the n-dodecyl to n-octadecyl derivatives displayed an enantiotropic SmA mesophase. Furthermore, the n-hexadecyl and n-octadecyl homologues exhibited a monotropic SmC mesophase transition during the cooling cycle. In the plot correlating transition temperature with the number of carbon atoms in the alkoxy chain, the Smectic A to nematic curve peaked, while the Smectic A to Smectic C transition (during cooling) displayed a declining trend. The N/SmA-isotropic curve followed the typical declining trend. All compounds exhibited UV activity and displayed photoluminescence in the blue emission region. Increased terminal chain length resulted in stronger emission and higher fluorescence quantum yield. Additionally, all compounds demonstrated moderate to good antioxidant activity. Theoretical chemical reactivity studies were conducted using DFT calculations, focusing on Frontier MOs and MEP mapping to determine energy gaps and areas of low and high electron density.

5.5. References:

[1] Ong L-K, Ha S-T, Yeap G-Y, et al. Heterocyclic pyridine-based liquid crystals: synthesis and mesomorphic properties. Liquid Crystals. 2018;**45**:1574–1584.

[2] Ali AJ, Karam NH. Synthesis and Characterization of Heterocyclic Compounds-Based Liquid Crystals. Journal of Medicinal and Chemical Sciences. 2023;**6**:827–833.

[3] Gao H, Zhang Q, Shreeve JM. Fused heterocycle-based energetic materials (2012–2019). J Mater Chem A. 2020;**8**:4193–4216.

[4] Kotian SY, Mohan CD, Merlo AA, et al. Small molecule based five-membered heterocycles: A view of liquid crystalline properties beyond the biological applications. Journal of Molecular Liquids. 2020;**297**:111686.

[5] Nagarajan R, Varadaraju C, Lee KH. Recent advancements in the role of N-Heterocyclic receptors on heavy metal ion sensing. Dyes and Pigments. 2021;**191**:109331.

[6] Mohammad Abu-Taweel G, Alharthi SS, Al-Saidi HM, et al. Heterocyclic Organic Compounds as a Fluorescent Chemosensor for Cell Imaging Applications: A Review. Critical Reviews in Analytical Chemistry. 2023;1–16.

[7] Yang Y, Forbes A, Cao L. A review of liquid crystal spatial light modulators: devices and applications. OES. 2023;**2**:230026–230029.

[8] Stolte M, Suraru S-L, Diemer P, et al. Diketopyrrolopyrrole Organic Thin-Film Transistors: Impact of Alkyl Substituents and Tolerance of Ethylhexyl Stereoisomers. Advanced Functional Materials. 2016;**26**:7415–7422.

[9] Madiahlagan E, B n S, Ngaini Z, et al. Synthesis, liquid crystalline properties and photo switching properties of coumarin-azo bearing aliphatic chains: Application in optical storage devices. Journal of Molecular Liquids. 2019;**292**:111328.

[10] NAGANO T. Development of fluorescent probes for bioimaging applications. Proc Jpn Acad Ser B Phys Biol Sci. 2010;**86**:837–847.

[11] Qu S, Lu Q, Wu S, et al. Two dimensional directed π–π interactions in a linear shaped bi-1,3,4-oxadiazole derivative to achieve organic single crystal with highly polarized fluorescence and amplified spontaneous emissions. J Mater Chem. 2012;**22**:24605–24609.

[12] Westphal E, Gallardo H, Sebastián N, et al. Liquid crystalline self-assembly of 2,5-diphenyl-1,3,4-oxadiazole based bent-core molecules and the influence of carbosilane end-groups. J Mater Chem C. 2019;**7**:3064–3081.

[13] Girotto E, Eccher J, Vieira AA, et al. Luminescent columnar liquid crystals based on 1,3,4-oxadiazole. Tetrahedron. 2014;**70**:3355–3360.

[14] Santos ABS, Manfredi AM, Salla CAM, et al. Highly luminescent liquid crystals by connecting 1,3,4-oxadiazole with thiazolo[5,4-d]thiazole units. Journal of Molecular Liquids. 2021;**321**:114887.

[15] Prabhu DD, Kumar NSS, Sivadas AP, et al. Trigonal 1,3,4-Oxadiazole-Based Blue Emitting Liquid Crystals and Gels. J Phys Chem B. 2012;**116**:13071–13080.

[16] Zhipeng M, Hongjun Y, Kun W, et al. Synthesis and Property of Unsymmetric Bent-core Liquid Crystals Based on 2,5-Disubstitueted-1,3,4-oxadiazole. Chinese Journal of Organic Chemistry. 2015;**35**:2575.

[17] Fouad FS, Khairuddean M, Twieg RJ. Diphenyl-1,3,4-oxadiazoles: synthesis and influence of side chain semifluorination and lateral ring fluorination on liquid crystalline properties. Molecular Crystals and Liquid Crystals. 2022;**732**:64–75.

[18] Carlsen PHJ, Jørgensen KB. Synthesis of unsymmetrically substituted 4H-1,2,4-triazoles. Journal of Heterocyclic Chemistry. 1994;**31**:805–807.

[19] Liras S, Allen MP, Segelstein BE. A Mild Method for the Preparation of 1,3,4-Oxadiazoles: Triflic Anhydride Promoted Cyclization of Diacylhydrazines. Synthetic Communications. 2000;**30**:437–443.

[20] Chiba T, Okimoto M. Electrooxidative cyclization of N-acylhydrazones of aldehydes and ketones to .DELTA.3-1,3,4-oxadiazolines and 1,3,4-oxadiazoles. J Org Chem. 1992;**57**:1375–1379.

[21] Lokanatharac KM, Linganna N, Hassner A, et al. A SIMPLE PROCEDURE FOR THE SYNTHESIS OF AMINOOXADIAZOLE. J of sci soc of thail. 1996;**22**:071.

[22] SELVARASU C, KANNAN P. Bent Shaped 1,3,4-Oxadiazole/Thiadiazole heterocyclic rings containing liquid crystals. J Chem Sci. 2015;**127**:1831–1838.

[23] Chudgar NK, Shah SN, Vora RA. Mesogenic Semicarbazones and Amino Oxadiazoles-I. Molecular Crystals and Liquid Crystals Incorporating Nonlinear Optics. 1989;**172**:51–56.

[24] Parra M, Alderete J, Zúñiga C, et al. Symmetric esters derived from 1,3,4-oxadiazole: synthesis, mesomorphic properties and structural study by semi-empirical calculations. Liquid Crystals. 2002;**29**:1375–1382.

[25] Kuo H-M, Li S-Y, Sheu H-S, et al. Symmetrical mesogenic 2,5-bis(6-naphthalen-2-yl)-1,3,4-thiadiazoles. Tetrahedron. 2012;**68**:7331–7337.

[26] He CF, Richards GJ, Kelly SM, et al. Heterocyclic polycatenar liquid crystals. Liquid Crystals. 2007;**34**:1249–1267.

[27] Mochizuki H, Hasui T, Kawamoto M, et al. Novel liquid-crystalline and amorphous materials containing oxadiazole and amine moieties for electroluminescent devices. Chemical Communications. 2000;1923–1924.

[28] Parra ML, Hidalgo PI, Elgueta EY. Synthesis and mesomorphic properties of oxadiazole esters derived from (R)-2-octanol, (S)-2-n-octyloxypropanol and (2S,3S)-2-chloro-3-methylpentanol. Liquid Crystals. 2008;**35**:823–832.

[29] Han J, Wang F-L, Zhang F-Y, et al. Synthesis, mesomorphic behaviour and photo-luminescent property of new mesogens containing 1,3,4-oxadiazole fluorophore. Liquid Crystals. 2010;**37**:1521–1527.

[30] Dingemans TJ, Samulski ET. Non-linear boomerang-shaped liquid crystals derived from 2,5-bis(p-hydroxyphenyl)-1,3,4-oxadiazole. Liquid Crystals. 2000;**27**:131–136.

[31] Apreutesei D, H. Mehl G. The design and investigation of laterally functionalised oxadiazoles. Journal of Materials Chemistry. 2007;**17**:4711–4715.

[32] Lehmann M, Köhn C, Kresse H, et al. Synthesis and properties of oxadiazole based V-shaped, shape persistent nematogens. Chem Commun. 2008;1768–1770.

[33] Hernández-Ainsa S, Barberá J, Marcos M, et al. Liquid Crystalline Ionic Dendrimers Containing Luminescent Oxadiazole Moieties. Macromolecules. 2012;**45**:1006–1015.

[34] Kim BG, Kim S, Park SY. Star-shaped discotic nematic liquid crystal containing 1,3,5-triethynylbenzene and oxadiazole-based rigid arms. Tetrahedron Letters. 2001;**42**:2697–2699.

[35] Cristiano R, Santos DMP de O, Gallardo H. Synthesis and characterization of low molecular mass luminescent liquid crystalline materials with 1,3,4-oxadiazole units. Liquid Crystals. 2005;**32**:7–14.

[36] Westphal E, Bechtold IH, Gallardo H. Synthesis and Optical/Thermal Behavior of New Azo Photoisomerizable Discotic Liquid Crystals. Macromolecules. 2010;**43**:1319–1328.

[37] Zhang P, Qu S, Wang H, et al. A new series of liquid-crystalline bi-1,3,4-oxadiazole derivatives: synthesis and mesomorphic behaviour. Liquid Crystals. 2008;**35**:389–394.

[38] Sato M, Ujiie S. New twin liquid crystalline diazole derivatives. Advanced Materials. 1996;**8**:567–569.

[39] Han J, Zhang M, Wang F, et al. Non-symmetric liquid crystal dimers based on 1,3,4-oxadiazole derivatives: synthesis, photoluminescence and liquid crystal behaviour. Liquid Crystals. 2010;**37**:1471–1478.

[40] Marin L, Damaceanu MD, Timpu D. New Thermotropc Liquid Crystalline Polyazomethines Containing Luminescent Mesogens. Soft Materials. 2009;**7**:1–20.

[41] Yang Q, Xu Y, Jin H, et al. A novel mesogen-jacketed liquid crystalline electroluminescent polymer with both thiophene and oxadiazole in conjugated side chain. Journal of Polymer Science Part A: Polymer Chemistry. 2010;**48**:1502–1515.

[42] Dave JS, Vora RA. Mesomorphic Behaviour of the Cholesteryl Esters-I: p-n-Alkoxybenzoates of Cholesterol. In: Johnson JF, Porter RS, editors. Liquid Crystals and Ordered Fluids. Boston, MA: Springer US; 1970. p. 477–487.

[43] Gupta RS. Synthesis of potential mesogens and study of their mesogenic properties [Internet]. The Maharaja Sayajirao University of Baroda; 1980. Available from: https://shodhganga.inflibnet.ac.in:8443/jspui/handle/10603/59388.

[44] Gray GW, Jones B. Mesomorphism and chemical constitution. Part II. The trans-p-n-alkoxycinnamic acids. J Chem Soc. 1954;1467–1470.

[45] Thaker BT, Kanojiya JB. Synthesis, Characterization and Mesophase Behavior of New Liquid Crystalline Compounds Having Chalcone as a Central Linkage. Molecular Crystals and Liquid Crystals. 2011;**542**:84/[606]-98/[620].

[46] Shriner RL, Hermann CKF, Morrill TC, et al. The Systematic Identification of Organic Compounds. John Wiley & Sons; 2003.

[47] Mahadeva J, Umesha KB, Rai KML, et al. Synthesis and Characterization of Mesogenic 1,3,4-Oxadiazole Derivatives. Molecular Crystals and Liquid Crystals. 2009;**509**:274/[1016]-282/[1024].

[48] Gim M-J, Beller DA, Yoon DK. Morphogenesis of liquid crystal topological defects during the nematic-smectic A phase transition. Nat Commun. 2017;**8**:15453.

[49] Jamain Z, Khairuddean M. Synthesis, Characterization and Determination of Mesophase Transition of Azo-azomethine Derivatives with Different Terminal Chain Lengths. Malaysian Journal of Chemistry. 2019;**21**:73–85.

[50] Sharma VS, Vekariya RH, Sharma AS, et al. Mesomorphic properties of liquid crystalline compounds with chalconyl central linkage in two phenyl rings. Liquid Crystals Today. 2017;**26**:46–54.

[51] Date RW, Imrie CT, Luckhurst GR, et al. Smectogenic dimeric liquid crystals. The preparation and properties of the α,ω-bis(4- *n* -alkylanilinebenzylidine-4′-oxy)alkanes. Liquid Crystals. 1992;**12**:203–238.

[52] Tandel RC, Patel NK. Synthesis and study of liquid crystalline properties of schiff's bases having 1,3,4-thiadiazole moiety. Liq Cryst. 2014;**41**:495–502.

[53] Abboud HJ, Lafta SJ, Tomi IHR. Synthesis and characterisation of asymmetrical mesogenic materials based on 2,5-disubstituted-1,3,4-oxadiazole. Liquid Crystals. 2017;**44**:2230–2246.

[54] Parra M, Hernandez S, Alderete J, et al. New Schiff's bases containing 1,3,4-thiadiazole and 1,3,4-oxadiazole units: a study of the effect of the heterocyclic ring and the position of the lateral alkoxy group on liquid crystalline properties. Liquid Crystals. 2000;**27**:995–1000.

[55] Pradhan B, Chakraborty N, Gupta RK, et al. Nonsymmetrical cholesterol dimers constituting regioisomeric oxadiazole and thiadiazole cores: an investigation of the structure–property correlation. New J Chem. 2017;**41**:879–888.

[56] Han J, Wang J, Zhang F, et al. Synthesis and mesomorphic behaviour of heterocycle-based liquid crystals containing 1,3,4-oxadiazole/thiadiazole and thiophene units. Liq Cryst. 2008;**35**:1205–1214.

[57] Han J, Chang X, Cao B, et al. Synthesis, Single Crystal Structures, and Liquid Crystal Property of 2,5-Diphenyl-1,3,4-Oxadiazoles/1,3,4-Thiadiazoles. Soft Materials. 2009;**7**:342–354.

[58] G.W. Gray. Molecular structure and the properties of liquid crystals [Internet]. London and New York: Academic Press; 1962. Available from: https://scholar.google.com/scholar_lookup?&title=Molecular%20Structure%20and%20the%20Properties%20of%20Liquid%20Crystals&publication_year=1962&author=Gray%2CGW.

[59] Sultana R, Arif R, Rana M, et al. 2-Amino-5-substituted-1,3,4-oxadiazole as chemosensor for Ni(II) ion detection: antifungal, antioxidant, DNA binding, and molecular docking studies. Luminescence. 2022;**37**:408–421.

[60] Mihailović N, Marković V, Matić IZ, et al. Synthesis and antioxidant activity of 1,3,4-oxadiazoles and their diacylhydrazine precursors derived from phenolic acids. RSC Adv. 2017;**7**:8550–8560.

[61] De Oliveira CS, Lira BF, Barbosa-Filho JM, et al. Synthetic Approaches and Pharmacological Activity of 1,3,4-Oxadiazoles: A Review of the Literature from 2000–2012. Molecules. 2012;**17**:10192–10231.

[62] Kumarasamy Y, Byres M, Cox PJ, et al. Screening seeds of some Scottish plants for free radical scavenging activity. Phytotherapy Research. 2007;**21**:615–621.

[63] Frisch M, Trucks G, Schlegel H, et al. Gaussian 09 (Revision A02). Gaussian Inc Wallingford CT. 2009;

[64] Pearson RG. Chemical hardness and the electronic chemical potential. Inorganica Chimica Acta. 1992;**198–200**:781–786.